Plant Communications
Research article

CellPress
Partner Journal

The plant cytosolic m^{6}A RNA methylome stabilizes photosynthesis in the cold

Alexandre Magno Vicente[1,5], Nikolay Manavski[1,5], Paul Torben Rohn[1], Lisa-Marie Schmid[1,6], Antoni Garcia-Molina[1,7], Dario Leister[1], Charlotte Seydel[2], Leo Bellin[3], Torsten Möhlmann[3], Gregor Ammann[4], Stefanie Kaiser[4] and Jörg Meurer[1,*]

[1]Plant Molecular Biology, Faculty of Biology, Ludwig-Maximilians-University Munich, Großhaderner Street 2-4, 82152 Planegg-Martinsried, Germany

[2]Plant Development, Faculty of Biology, Ludwig-Maximilians-University Munich, Großhaderner Street 2-4, 82152 Planegg-Martinsried, Germany

[3]Plant Physiology, Faculty of Biology, University of Kaiserslautern, Erwin-Schrödinger-Street, 7, 67663 Kaiserslautern, Germany

[4]Pharmaceutical Chemistry, Goethe University Frankfurt, Max-von-Laue-Str. 9, 60438 Frankfurt am Main, Germany

[5]These authors contributed equally to this article.

[6]Present address: Loewe Biochemica GmbH, Mühlweg 2a, 82054 Sauerlach, Germany

[7]Present address: Center for Research in Agricultural Genomics, 08193 Cerdanyola Barcelona, Spain

***Correspondence: Jörg Meurer (meurer@bio.lmu.de)**

https://doi.org/10.1016/j.xplc.2023.100634

ABSTRACT

The sessile lifestyle of plants requires an immediate response to environmental stressors that affect photosynthesis, growth, and crop yield. Here, we showed that three abiotic perturbations—heat, cold, and high light—triggered considerable changes in the expression signatures of 42 epitranscriptomic factors (writers, erasers, and readers) with putative chloroplast-associated functions that formed clusters of commonly expressed genes in *Arabidopsis*. The expression changes under all conditions were reversible upon deacclimation, identifying epitranscriptomic players as modulators in acclimation processes. Chloroplast dysfunctions, particularly those induced by the oxidative stress-inducing norflurazon in a largely GENOME UNCOUPLED-independent manner, triggered retrograde signals to remodel chloroplast-associated epitranscriptomic expression patterns. N^6-methyladenosine (m^{6}A) is known as the most prevalent RNA modification and impacts numerous developmental and physiological functions in living organisms. During cold treatment, expression of components of the primary nuclear m^{6}A methyltransferase complex was upregulated, accompanied by a significant increase in cellular m^{6}A mRNA marks. In the cold, the presence of FIP37, a core component of the writer complex, played an important role in positive regulation of thylakoid structure, photosynthetic functions, and accumulation of photosystem I, the Cytb_6f complex, cyclic electron transport proteins, and Curvature Thylakoid1 but not that of photosystem II components and the chloroplast ATP synthase. Downregulation of FIP37 affected abundance, polysomal loading, and translation of cytosolic transcripts related to photosynthesis in the cold, suggesting m^{6}A-dependent translational regulation of chloroplast functions. In summary, we identified multifaceted roles of the cellular m^{6}A RNA methylome in coping with cold; these were predominantly associated with chloroplasts and served to stabilize photosynthesis.

Key words: m^{6}A, RNA methylation, cold acclimation, stress response, *Arabidopsis thaliana*, photosynthesis, chloroplast

Vicente A.M., Manavski N., Rohn P.T., Schmid L.-M., Garcia-Molina A., Leister D., Seydel C., Bellin L., Möhlmann T., Ammann G., Kaiser S., and Meurer J. (2023). The plant cytosolic m^{6}A RNA methylome stabilizes photosynthesis in the cold. Plant Comm. **4**, 100634.

INTRODUCTION

Natural environmental fluctuations can cause unfavorable temperatures, light levels, and water accessibility that negatively

Published by the Plant Communications Shanghai Editorial Office in association with Cell Press, an imprint of Elsevier Inc., on behalf of CSPB and CEMPS, CAS.

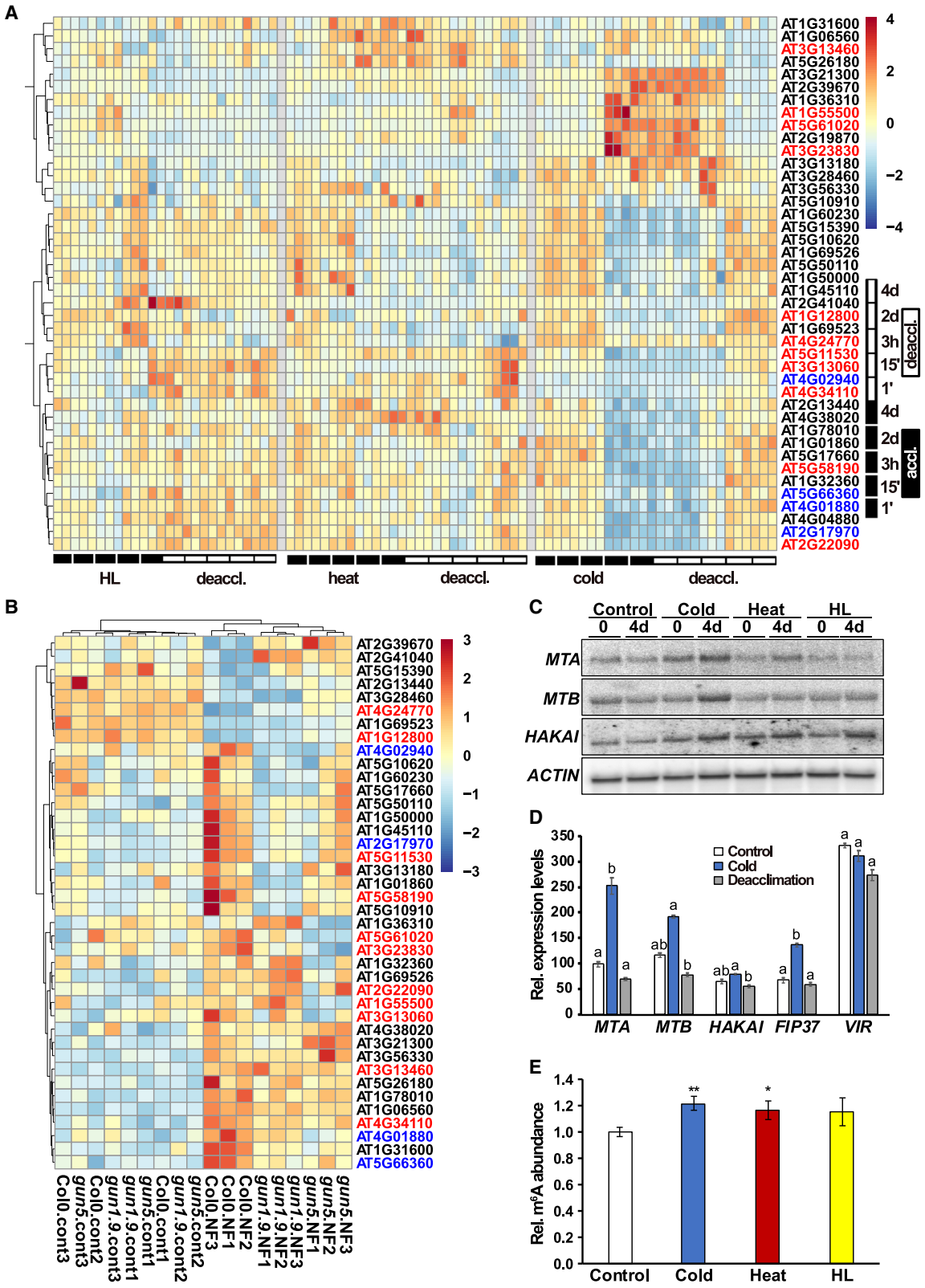

Figure 1. Changes in transcript levels of writers, erasers, and readers during acclimation to high light, heat, and cold followed by deacclimation.

(A and B) Heatmaps with hierarchical clustering of transcript values for chloroplast-associated epitranscriptomic players (writers, erasers, and readers in black, blue, and red, respectively) were elaborated according to the Ward d2 method using **(A)** z-means of plants (de)acclimated to high light, heat, and

(legend continued on next page)

affect plants on multiple levels, such as growth, development, and photosynthesis. In addition to regulation of gene expression, mechanisms of posttranscriptional regulation at the RNA and protein levels represent important layers in the control of plant responses to adverse environmental conditions (Chinnusamy et al., 2007; Nakaminami and Seki, 2018). Therefore, a complex response to stressors must also be tightly regulated at multiple levels. Notably, many of these reactions involve chloroplasts, which constantly act as environmental sensors and targets of challenging and ever-changing conditions (Crosatti et al., 2013; Crawford et al., 2018; Manavski et al., 2018; Kleine et al., 2021; Schwenkert et al., 2021). Nonetheless, the molecular mechanisms used to overcome these challenges are far from being fully understood.

Posttranscriptional RNA modifications are widespread in living organisms, and over 170 types of chemical modification have been identified to date (Boccaletto et al., 2021). Regulatory proteins that install (writers), remove (erasers), and interpret (readers) such marks in a site-specific manner are involved in these epitranscriptomic modifications (Manavski et al., 2021a). By affecting RNA stability, splicing, transport, assembly, interactions, and translation, these modifications modulate the fate of numerous coding and non-coding RNAs (Shi et al., 2020). N^6-methyladenosine (m^{6}A) is considered the most common internal modification in eukaryotic mRNAs. Importantly, m^{6}A methylation marks are known to be pervasive in nucleus-derived mRNAs related to chloroplast categories and are also highly enriched in chloroplast mRNAs (Luo et al., 2014; Wang et al., 2017; Manavski et al., 2021a; Qin et al., 2022).

In plants, the major and conserved nuclear m^{6}A writer complex contains the two annotated methyltransferases MTA and MTB, the methylation factor VIRILIZER (VIR), the conserved E3 ubiquitin ligase-like HAKAI, and the central component FIP37 (Shen et al., 2016; Růžička et al., 2017; Shen, 2023). With the exception of HAKAI, other null alleles of this writer complex are arrested at the globular stage of embryonic development (Růžička et al., 2017).

Besides developmental processes, m^{6}A is also linked to biotic and abiotic stress responses in living organisms (Liang et al., 2020: Manavski et al., 2021a; Yu et al., 2021). For example, under salt stress, m^{6}A marks protect several transcripts related to salt and osmotic stress response from degradation in *Arabidopsis* (Anderson et al., 2018). Accordingly, m^{6}A writer mutants also displayed salt-sensitive phenotypes (Hu et al., 2021). Under heat, responsive transcripts are relocated to stress granules by the m^{6}A reader ECT2, potentially playing a role in RNA stability and translation (Scutenaire et al., 2018). VIR has been shown to impact various plant developmental programs and has a positive effect on photosynthesis under high light (Růžička et al., 2017; Zhang et al., 2022). Despite rapid progress in plant research on m^{6}A-methylation marks, their importance for coping with environmental changes has only recently been explored (Manavski et al., 2021a; Zhang et al., 2022).

Here, we show that genes encoding 42 mostly uncharacterized epitranscriptomic factors with putative chloroplast function and/or localization were reversibly differentially expressed in response to perturbations by heat, high light, and cold and that they responded to the functional state of the chloroplast largely independently of Genome Uncoupled (GUN)1 and GUN5. Moreover, we show that both expression of components of the major m^{6}A writer complex and cellular m^{6}A mRNA methylation marks increased under cold acclimation and that FIP37, as a major component of the writer complex, was important for maintaining efficient photosynthesis and other chloroplast functions. Thus, we identified the cellular m^{6}A RNA methylome as a central and multifaceted hub important for stabilizing functional photosynthesis in the cold and revealed the chloroplast as the main player in addressing cold response.

RESULTS

Expression of genes encoding chloroplast-associated epitranscriptomic factors is responsive to cold, heat, high light, and the functional state of the chloroplast

Previous transcriptome-wide maps have revealed the involvement of m^{6}A in developmental processes and certain plant stress responses (Shen et al., 2016; Anderson et al., 2018; Hu et al., 2021; Qin et al., 2022). Because the chloroplast appears to play a crucial role as a sensor of environmental changes (Kleine et al., 2021), we selected 42 annotated and largely uncharacterized epitranscriptomic players (writers, erasers, and readers) from *Arabidopsis* databases that were either potentially associated with chloroplast functions and/or located within this organelle (Supplemental Table 1). We then investigated the expression behavior of these factors upon 4-day cold, heat, and high light treatments, conditions under which we recently observed global transcriptomic changes (Garcia-Molina et al., 2020). Normalized transcript values were used to create a heatmap with hierarchical clustering to capture overall expression patterns. Remarkably, heatmaps showed that all 42 selected genes displayed changes in transcript abundance in at least one of the three treatments (Figure 1A). Depending on the condition, transcripts formed clusters of co-expressed genes that were either up- or downregulated, suggesting coordinated

cold treatments for 4 days as reported recently (Garcia-Molina et al., 2020) or **(B)** *Z* scores of normalized 5-day-old WT (Col0), *genome uncoupled* (*gun*) *1-9*, and *gun5* mutant seedlings under control or norflurazon treatment as reported by Koussevitzky et al. (2007).
(C) RNA gel blot analysis of selected genes of the m^{6}A writer complex in the WT before and after 4 days of cold, heat, and high light treatment using 8 μg leaf RNA. An actin probe was used as the loading control.
(D) Reversibility of upregulation of genes encoding m^{6}A writer components during deacclimation, as revealed by RNA sequencing analysis. Bar plots depict means ± standard deviation for normalized counts of selected transcripts in pretreated, cold-treated, and deacclimated plants at day 4. Statistical significance was tested by one-way ANOVA with post hoc Tukey's honestly significant difference (HSD) test ($p \leq 0.05$).
(E) Quantification of m^{6}A marks in poly(A)-enriched RNA samples using LC–MS. m^{6}A abundance was normalized to that of the control for each sample (n = 5), and statistical significance among treatments was determined using one-way ANOVA and Tukey's HSD post hoc test (*$p \leq 0.05$; **$p \leq 0.01$). Normalization to the control was performed for each sample.

control during acclimation and an important link between epitranscriptomic marks and chloroplast perception of external stimuli. Importantly, the expression levels of all players returned to levels of the previous standard conditions within 4 days of deacclimation, suggesting that the factors are indeed directly involved in the acclimation response (Figure 1A).

It is tempting to assume that the chloroplast itself plays a central role in regulating m^{6}A methylation because it is generally thought to sense environmental changes that can trigger retrograde signals (Kleine et al., 2021). To investigate the relevance of chloroplast signaling for the cellular m^{6}A-methylation machinery, transcript levels of 40 epitranscriptomic factors under standard conditions were compared with those of norflurazon (NF)-treated wild-type (WT), *gun1-9*, and *gun5* mutant seedlings (Koussevitzky et al., 2007) (Figure 1B). The heatmap depicted two main trends corresponding to core sets of transcripts that tended to be either down- (upper 8 transcripts) or upregulated (remaining transcripts) upon NF treatment. Interestingly, transcript levels of the selected genes displayed similar values under standard conditions for all three genotypes, indicating that most genes responded to the functional state of the chloroplast largely independently of GUN1 and GUN5 proteins. The degree of induction or repression upon NF treatment changed only partially in both *gun* mutants compared with the WT (Figure 1B). Thus, expression of the epitranscriptomic factors is also responsive to the functional state of the chloroplast, but *gun1-9* and *gun5* do not markedly affect this communication for most genes.

Given that m^{6}A is the most frequent RNA modification, we examined gene expression of three representative members of the main nuclear m^{6}A writer complex, *MTA*, *MTB*, and *HAKAI*, using RNA gel blot analysis under control conditions and the three treatments (Figure 1C). Interestingly, expression of *MTA*, *MTB*, and *HAKAI* was upregulated after 4 days of cold treatment. *HAKAI* also showed increased expression under high light treatment, and both *HAKAI* and *MTA* showed increased expression in response to heat. Thus, our results suggest an individual response of the components of the m^{6}A writer complex to all three environmental conditions and, in particular, a concerted activation of the three components under cold. To corroborate these data under cold conditions and verify the ability to deacclimate, we retrieved expression data for the five components of the writer complex from our previous transcriptomic study (Garcia-Molina et al., 2020) (Figure 1D). Indeed, expression of *MTA*, *MTB*, *HAKAI*, and *FIP37* was clearly increased after cold treatment, whereas that of *VIR* showed little change. Again, expression fell to levels of pretreated plants within 4 days after transfer to standard conditions, indicating deacclimation of the cold response. These data confirm the important role of the writer complex as a modulator of the acclimation response, with individual contributions of its components.

m^{6}A methylation of mRNAs in *Arabidopsis* increases in the cold

Because our results demonstrated that expression of genes encoding components of the major nuclear m^{6}A writer complex and other chloroplast-associated epitranscriptomic players is increased upon cold treatment, it is reasonable to assume that m^{6}A marks of cellular mRNAs also increase during cold acclimation. Absolute quantification of m^{6}A requires normalization to the amount of injected RNA, and highly abundant tRNAs and rRNAs were therefore carefully removed prior to our liquid chromatography with mass spectrometry (LC–MS) analysis. tRNAs were removed through size-exclusion chromatography, whereas long RNA fractions were rRNA depleted through poly(A) enrichment. Quality assurance of poly(A) fractions was performed by automated gel electrophoresis (Supplemental Figure 1). Notably, the m^{6}A content of poly(A) RNAs was significantly enriched by approximately 20% in cold- and heat-treated samples compared with control plants (Figure 1E). The observed increase in m^{6}A under high light was not statistically relevant. It should be noted that the increase in m^{6}A represents the sum of up- and downregulated m^{6}A methylations and that different sites and transcripts are likely to be targeted for m^{6}A methylation under the three chosen conditions. In this regard, recent studies have performed GO analysis of cold-treated WT and m^{6}A mutant plants and provided the sequence context of m^{6}A marks (Govindan et al., 2022; Wang et al., 2023). This is all consistent with the fact that the m^{6}A-methylation pattern in heat and cold is associated with the activation of heat- and cold-sensitive genes, respectively, suggesting that different transcripts and sites are labeled with m^{6}A under different conditions (Figure 1A) (Govindan et al., 2022; Wang et al., 2022). In summary, upregulation of m^{6}A mRNA labeling in cold is congruent with increased cold-dependent expression of genes encoding components of the nuclear m^{6}A writer complex (Figures 1C–1E).

Writer mutants are sensitive to cold

Photosynthesis is the main biological process for capturing light energy to form carbohydrates and is strongly affected by exposure to cold (Theocharis et al., 2012; Kleine et al., 2021). Because the m^{6}A content of mRNAs was considerably enriched in *Arabidopsis* under cold, we next investigated how previously described mutants of individual subunits of the major writer complex and corresponding complemented lines behaved under this condition (Shen et al., 2016; Růžička et al., 2017; Qin et al., 2022; Shen, 2023; Wong et al., 2023). Hypomorphic alleles of *FIP37*, *VIR*, and *MTA* showed a decrease in m^{6}A levels to about 10%–15%, and the *hakai* knockout decreased to about 65% (Růžička et al., 2017; Parker et al., 2020). We initially measured photosystem II (PSII) integrity (Fv/Fm) of the four *fip37-4*, *mta*, *vir-1*, and *hakai* mutant lines of the m^{6}A writer complex during cold acclimation. None of the mutant lines showed a marked decrease in the maximum quantum yield of PSII, measured as Fv/Fm under standard conditions, indicating that photosynthesis was not primarily impaired in the mutants (Figure 2A). However, Fv/Fm decreased much faster in these lines than in the WT just a few hours after cold exposure (Figure 2A). After 16 h of cold acclimation, Fv/Fm stagnated at about 0.7 in the WT, whereas it still showed a continuous decline within the first 4 days in the mutants (Figure 2B). The complemented *vir1* and *fip37-4* mutant lines (referred to here as *vir-1c* and *fip37-4c*) performed much better than the single mutants but failed to fully recover the Fv/Fm level, indicating incomplete complementation, probably due to the presence of C-terminal hemagglutinin tags in both lines, which could slightly affect the stability of the writer complex with functional interdependent subunits (Shen, 2023). Because the strongest effect of cold on Fv/Fm was

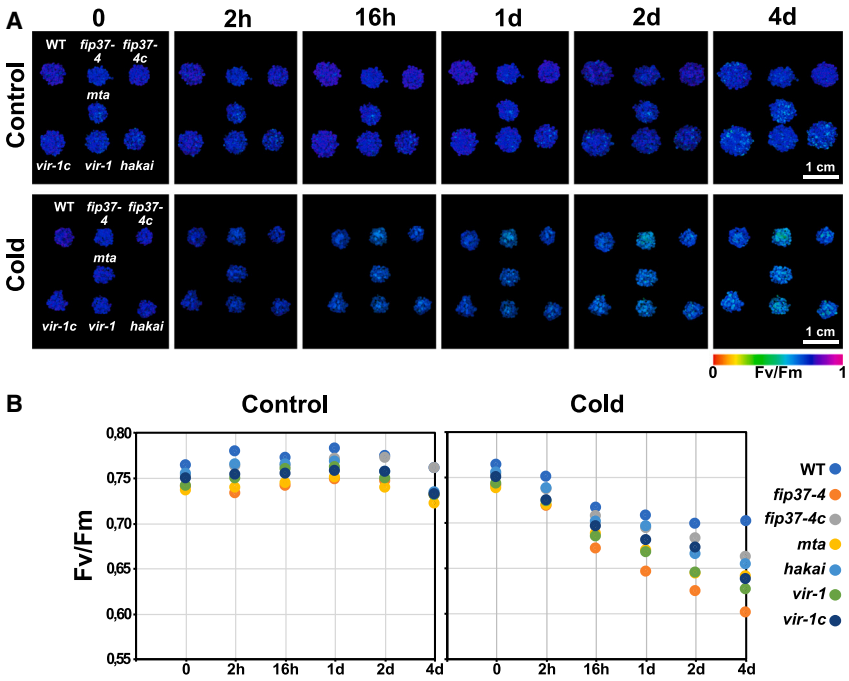

Figure 2. Photosynthetic performance of m^{6}A writer complex mutants is negatively affected by cold treatment.

(A) Imaging of Fv/Fm values for the WT, knockdowns (*fip37-4*, *mta*, *vir-1*, *hakai*), and corresponding complemented lines (*fip37-4c*, *vir-1c*) grown for 10 days on medium. Scale bar: 1 cm.

(B) Fv/Fm data were collected at several time points of cold treatment as indicated. The corresponding numeric Fv/Fm values reflect the cold sensitivity of the writer mutants.

observed for *fip37-4* (Figure 2), we took a closer look at FIP37 to obtain a comprehensive picture of the writer complex and its specific role in cold acclimation.

If FIP37 were indeed involved in cold acclimation, we would expect the effects of cold on photosynthesis to be reversible in the corresponding mutant. Indeed, after cold treatment, *fip37-4* plants were completely deacclimated upon exposure to standard conditions for another 4 days (Supplemental Figure 2). Taken together, these results suggest that the activity of the writer complex plays a distinct role in facilitating efficient photosynthesis under cold acclimation. Importantly, the fact that Fv/Fm values returned to levels of pretreated leaves within 4 days demonstrates that FIP37, and presumably the entire m^{6}A writer complex, is a true acclimation factor or modulator (Kleine et al., 2021).

Photosynthetic efficiency is severely decreased in *fip37-4* in the cold

We next investigated the effect of cold on defined photosynthetic parameters in the *fip37-4* mutant to identify the primary deficiencies. Chlorophyll content, Fv/Fm, the efficient quantum yield of PSII (Φ(II)), non-photochemical quenching (Φ(NPQ)), and the non-regulated, basal non-photochemical energy loss in PSII (Φ(NO)) were not markedly changed under standard growth conditions in the mutant (Figure 3A and Supplemental Figures 2 and 3). In the cold, chlorophyll fluorescence of *fip37-4* remained at higher levels during induction and decreased only slowly compared with that of the WT (Supplemental Figure 3A). This behavior is indicative of mutants with a defective electron transport chain or PSI (Meurer et al., 1996). After cold exposure, Fv/Fm and Φ(II) values were severely decreased in *fip37-4* compared with WT (0.54 vs. 0.70 and 0.12 vs. 0.28, respectively), whereas Φ(NPQ) remained largely unchanged in all samples (Figure 3A). Φ(NPQ), however, increased slowly compared with the values of WT and *fip37-4c*, indicating that cold-treated *fip37-4* was unable to properly regulate photosynthesis after the sudden onset of light (Supplemental Figure 3B). As expected, Φ(NO) levels increased in all samples in the cold, with the highest value in the mutant (0.49 vs. 0.67), indicating elevated oxidative pressure (Figure 3A). We concluded that cold treatment has a drastic and rapid effect on photosynthetic electron transport, causing increased oxidative damage in the mutant. In agreement with the PSII measurements, we found no changes in the activity of PSI under standard conditions. All three parameters, photosystem I yield (Φ(I)) and the donor and acceptor side limitations, Φ(ND) and Φ(NA), were apparently unaffected in the mutant (Figure 3B). In the cold, however, the ∼25% decrease in Φ(I) was due primarily to a four-fold increase in limitation on the donor side but not on the acceptor side, again suggesting that electron flow toward PSI is greatly reduced in cold-treated *fip37-4* mutants (Figure 3B).

FIP37 deficiency affects accumulation of chlorophyll and specific photosynthetic complexes in the cold

We next wanted to determine whether cold treatment also affects chloroplast pigment and protein content. Chlorophyll levels in *fip37-4* were reduced only in the cold to 86.68% ± 5.67% compared with those in the WT. Representative subunits of major thylakoid membrane complexes were examined by immunoblot analysis. Under standard conditions, there was a marginal decrease in all analyzed subunits of PSI (PsaA, PsaD, PsaO, PsaO), PSII (PsbA, PsbD, PsbO, LhcB6), the Cytb_6f complex (Cyt*f*, Cytb_6), ATP synthase (AtpB), and the cyclic electron transport (CET) (PGR5, PGRL1, NdhB) in *fip37-4* compared with the WT (Figure 4A). After a 4-day cold treatment, levels of proteins were generally slightly decreased in the WT. However, the decrease in protein levels of PSI (PsaA, PsaO), the Cytb_6f complex, and the CET (PGRL1, NdhB) was much more pronounced in *fip37-4* (Figure 4A). Levels of PSII and ATP synthase proteins and of PGR5 were comparable in cold-treated WT and mutant plants, indicating a specific deficiency in thylakoid membrane complexes. Furthermore, levels of CurT1, which is required for curvature of the thylakoid membrane (Armbruster et al., 2013), were also decreased after exposure to 4°C.

Expression of photosynthetic transcripts is changed in cold-treated *fip37-4*

We next asked whether protein levels are determined by mRNA levels and examined the expression of representative plastid and nuclear genes from PSI (*PsaA*, *PsaD*, *PsaL*, *PsaO*), the Cytb_6f

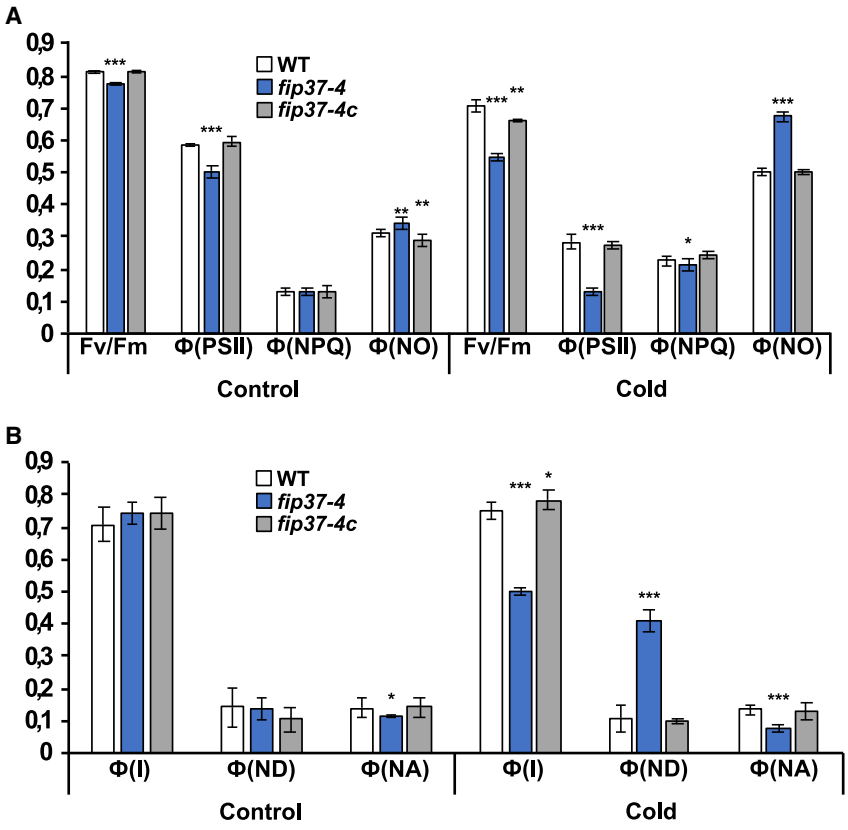

Figure 3. Cold-induced photosynthetic deficiency in *fip37-4*.
(A) The photosynthetic parameters Fv/Fm, Φ(II), Φ(NPQ), and Φ(NO) were calculated from plants grown in soil for 14 days under standard conditions and then subjected to 4 days of cold treatment.
(B) PSI parameters Φ(I), Φ(ND), and Φ(NA) were calculated from plants grown as described in **(A)**.
Statistically significant differences compared with the control condition were assessed using Student's *t*-tests in **(A)** and **(B)** (*p ≤ 0.05; **p ≤ 0.01; ***p ≤ 0.001).

complex (*PetB*, *PetC*), and PSII (*PsbA*, *PsbO1*, *PsbO2*). Whereas levels of *petC* and *psaL* transcripts were severely downregulated in the cold in both WT and *fip37-4*, expression of all other genes was comparable under standard and cold conditions. Under control and cold conditions, levels of nuclear- (*psaO*, *psbO1*, *psaD*) and plastid-derived (*psaA*, *psbA*, *petB*) transcripts were slightly higher and lower, respectively, in *fip37-4* than in the WT (Figure 4B). Strikingly, expression of *PsbO2* and *PetC* was considerably upregulated in *fip37-4* under standard conditions but returned to lower levels after cold treatment. However, levels of cytoplasmic transcripts still remained higher in *fip37-4* than in the WT, presumably to compensate for protein deficiencies.

As has often been observed in mutants not directly affected in chloroplast RNA metabolism, slight changes in processed *petB* transcripts occurred between WT and *fip37-4* (Figure 4B). Thus, we conclude that the observed differences in gene expression do not correlate with the decreases in the set of proteins, emphasizing that posttranscriptional changes are responsible for the observed deficiencies in protein levels.

Cytoplasmic translation is reduced in cold-treated *fip37-4*

In contrast to those associated with most other GO terms, the cold-enriched m^{6}A peaks of cytoplasmic transcripts associated with photosynthesis and chloroplast organization showed preferentially lower ribosome loading (Govindan et al., 2022), presumably explaining the decreased levels of most investigated nuclear-encoded proteins in WT plants in the cold (Figure 4). We therefore examined ribosomal occupancy of photosynthetic transcripts with altered levels in *fip37-4* in the cold (Figure 5A). No obvious differences between WT and *fip37-4* were observed for general ribosomal loading of chloroplast transcripts, including *psaA*. However, methylene blue staining of the polysome fractions showed that, in contrast to WT, a substantial proportion of cytoplasmic 25S and 18S ribosomes was found in monosomes in *fip37-4* in the cold. To examine whether polysome loading of nuclear-derived photosynthetic transcripts was affected, we probed fractions with *psaD* and *psaL*. In WT and *fip37-4*, both transcripts were found mainly in high-molecular-weight polysomes in the cold; however, in *fip37-4*, some of these transcripts were also present in monosomes (Figure 5A). This is also consistent with reduced PsaD and PsaL protein levels in cold-treated *fip37-4* plants and suggests a mechanism by which translation of even upregulated nucleus-derived transcripts with photosynthetic functions is downregulated owing to the deficiency of most m^{6}A marks.

To examine translation further, we performed *in vivo* labeling experiments using cycloheximide and chloramphenicol as inhibitors of cytoplasmic and chloroplast translation, respectively (Figure 5B). The data clearly indicated that general chloroplast translation remained unchanged in the *fip37-4* mutant, whereas overall cytoplasmic translation was downregulated by approximately 50% when comparing protein loading. This finding confirms that reduced cytoplasmic translation of RNAs encoding chloroplast proteins is likely to be the cause of the observed deficits in plastid proteins in *fip37-4*. In addition, unchanged protein biosynthesis in chloroplasts suggests that decreased plastid-encoded proteins are unstable owing to the reduced amount of specific nuclear-encoded chloroplast proteins constituting the same photosynthetic complexes.

Assembly studies of photosynthetic complexes

In addition to steady-state levels of proteins, the assembly of photosynthetic thylakoid membrane complexes was analyzed by blue native PAGE using extracts from *fip37-4* and WT plants exposed to cold (Supplemental Figure 4). The overall assembly of complexes did not appear to be affected. Immunological analysis of the second dimension showed that levels of all

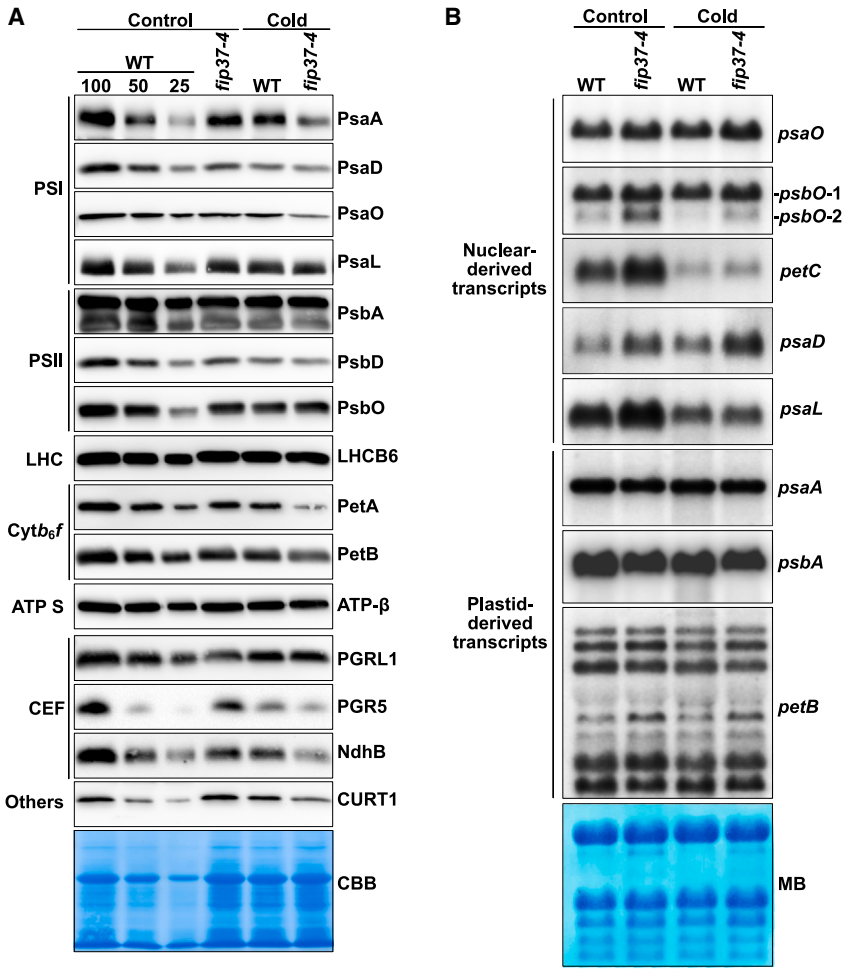

Figure 4. Accumulation of photosynthetic proteins and RNAs in FIP37-deficient plants.
(A) Steady-state levels of representative subunits of photosynthetic complexes. Immunoblot analyses were performed with plants grown for 10 days under standard conditions and an additional 4 days under cold conditions. Coomassie brilliant blue staining served as a loading control. ATP S, ATP synthase.
(B) RNA gel blot analysis of plastid- and nuclear-derived transcripts encoding chloroplast proteins in WT and *fip37-4* under control and cold conditions. 3 μg total RNA was loaded. Methylene blue was used as a loading control.

detectable PSII complexes and D1 appeared comparable in *fip37-4* and the WT. However, when using equal chlorophyll loading, the mutant exhibited decreased levels of the PSI proteins PsaA and PsaG, as well as reduced levels of Cytb_6 in the more prominent dimeric Cytb_6f complexes compared with monomers (Supplemental Figure 4).

Role of FIP37 in thylakoid organization in the cold

CurT1 complexes are highly enriched in grana stacks and are required for the curvature, and thus the architecture, of the thylakoid membrane (Armbruster et al., 2013). Because levels of the CurT1 protein appeared to be severely reduced in cold-acclimated *fip37-4* mutants compared with the WT, we attempted to examine the ultrastructure of the chloroplast. For this, chloroplasts from 14-day-old seedlings were analyzed by transmission electron microscopy before and after 4 days of cold treatment. Under standard conditions, chloroplasts from both WT and *fip37-4* had intact plastids and parallel-running thylakoid membranes with well-defined grana stacks, indicating that reduced levels of FIP37 at 22°C had no obvious effect on chloroplast ultrastructure (Figure 6). However, after cold treatment, thylakoids in *fip37-4* were organized in a wavy manner, and grana stacks consisted of fewer membrane layers, similar to those of *curt1* mutants, whereas the WT maintained a similar ultrastructure compared with standard conditions (Figure 6). Reduced levels of CurT1 supported the ultrastructural changes and strongly indicated that FIP37, in addition to its association with photosynthesis and cold acclimation, may potentially be involved in a broader range of chloroplast functions.

FIP37 deficiency induces ROS formation in the cold

Chloroplasts can produce reactive oxygen species (ROS) under hostile environmental conditions via both photosystems (Li and Kim, 2021), and we therefore examined ROS formation after cold treatment (Figure 7A). Nitro blue tetrazolium (NBT) and 3,3′-diaminobenzidine (DAB) stains, which detect O_2^- and H_2O_2, respectively, revealed no differences among the WT, *fip37-4*, and *fip37-4c* under standard conditions at 22°C. However, transfer to cold resulted in more intense staining with both dyes in the *fip37-4* mutant compared with the WT and *fip37-4c*, indicating an increased oxidative burst (Figure 7A).

Because of the oxidative stress to which the mutants were exposed in the cold, expression of ROS-related genes was monitored by qRT–PCR. In the cold, expression of the ROS-responsive transcription factors *ZAT12* and *ZAT10* was significantly increased in *fip37-4* (Figure 7B). The transcript level of superoxide dismutase showed an increase in all tested lines but no marked differences between WT and *fip37-4* in the cold. Expression of ascorbate peroxidase1 was upregulated under both standard and cold conditions in the mutant (Figure 7). Overall, these results suggest that ROS formation in plants with lower FIP37 levels increased under cold conditions, although the ability to respond to oxidative stress with the induction of cold-responsive genes was not impaired.

Anthocyanin production is absent in cold-treated *fip37-4*

Anthocyanins are secondary metabolites that accumulate in response to pathogen attack and cold, as well as UV and strong light, suggesting a possible role in plant tolerance to various environmental conditions (Winkel-Shirley, 2002; Xu and Rothstein, 2018). However, the molecular mechanism by which anthocyanins

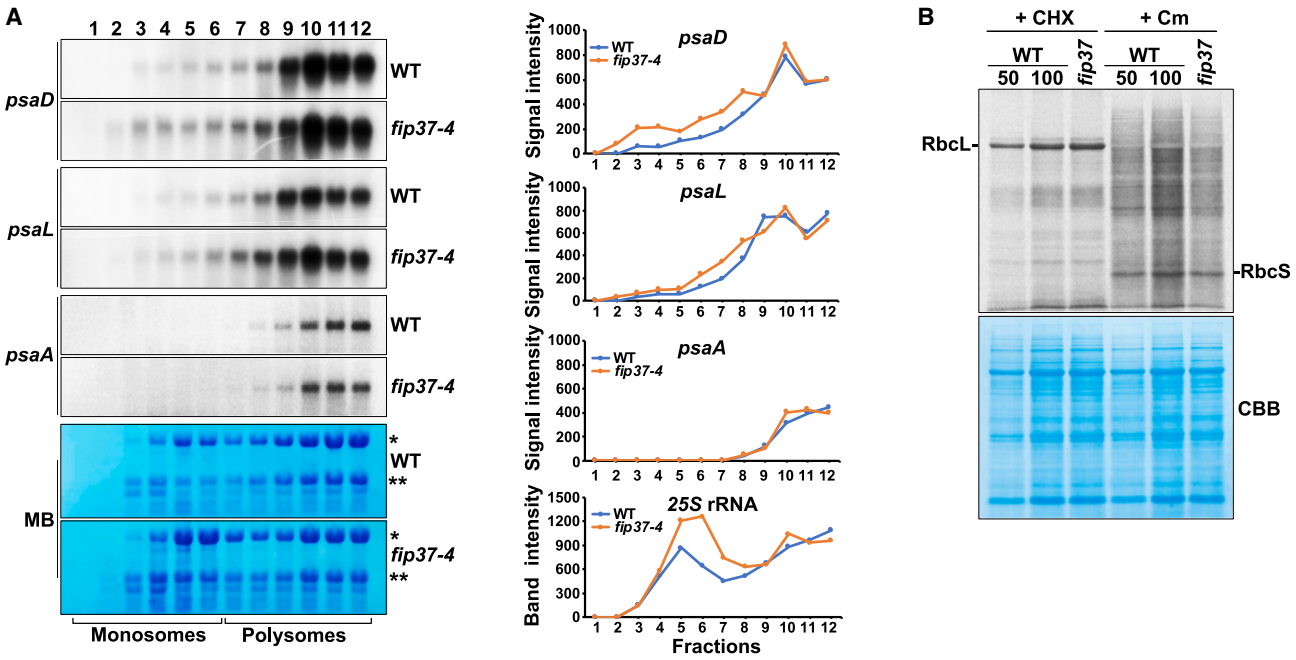

Figure 5. Polysome loading and *in vivo* radiolabeling of cytoplasmic and chloroplast proteins.

(A) Separation of intact polysomes fractionated by ultracentrifugation. Fractions were stained with methylene blue. Monosomal and polysomal fractions are indicated. Isolated RNA was denatured and subjected to gel blot analysis using *psaA*, *psaD*, and *psaL* probes. The signal intensity of the fractions is represented graphically on the right side. MB, methylene blue.

(B) Cytoplasmic and chloroplast proteins were freshly radiolabeled in the presence of chloramphenicol or cycloheximide, respectively. *In vivo* labeled proteins were subjected to SDS–PAGE. RbcL and RbcS bands are indicated in the chloroplast and cytosolic labels, respectively. Asterisks show the cytoplasmic 25S (*) and the 18S (**) rRNAs. Coomassie brilliant blue staining was used as a loading control. CHX, cycloheximide; Cm, chloramphenicol.

protect photosynthetic leaves against external stressors is still enigmatic (Araguirang and Richter 2022). The purple leaf phenotype observed in the WT and *fip37-4c* was based on anthocyanin accumulation, which was clearly absent in *fip37-4* in the cold (Supplemental Figure 5A). The anthocyanin content was calculated to be reduced to less than 20% in *fip37-4* compared with the WT and *fip37-4c* under cold conditions (Supplemental Figure 5B). Increased ROS production is thought to suppress flavonoid biosynthesis, and synthesis of sucrose and triose phosphate is known to be a prerequisite for anthocyanin production mediated by transcription factors (Richter et al., 2020). Reduced photosynthetic efficiency and increased ROS production in *fip37-4* could therefore be responsible for the lack of anthocyanins in the cold.

The *fip37-4* mutant is responsive to cold

To investigate whether a lack of induction of cold-responsive genes could explain the *fip37-4* phenotype, we further tested the expression of known genes associated with cold shock response and cold acclimation. C-repeat-binding factors play important roles in plant acclimation to cold (Liu et al., 2019). These factors bind to the C-repeat responsive element motif found in promoters of cold-responsive (*COR*) genes such as *COR15A* and *RD29A*. Cold-triggered induction of *C-repeat-binding factor 2*, *COR15A*, and *RD29A* expression in *fip37-4* was comparable to that in the WT, albeit somewhat delayed (Supplemental Figure 6). Thus, *fip37-4* did not lose its ability to induce the expression of genes important for cold acclimation, suggesting that reduced m^{6}A methylation has little or no effect on the cold response of the studied genes.

In conclusion, our results suggest that downregulation of FIP37 has no particular effect on photosynthesis under standard conditions but is crucial for efficient photosynthesis and other chloroplast functions related to plant growth, viability, and fitness during cold acclimation.

DISCUSSION

The identification of molecular components that mediate plant acclimation to adverse environmental conditions is an important and timely task in plant biology and breeding programs. Regardless of their nature, effects of perturbations on plants always take place on multiple levels, such as growth, development, and photosynthetic functions (Li et al., 2022). This implies that acclimation factors that allow plants to better cope with stress must also act at multiple levels. It is therefore tempting to speculate that methylation of different mRNAs at defined positions makes a significant contribution to such multifactorial responses during acclimation processes (Manavski et al., 2021a). Indeed, RNA methylation introduced by m^{6}A writer proteins is emerging as an essential posttranscriptional mechanism of gene regulation in plant responses to (a)biotic stresses and developmental stages. The potential role of writers, erasers, and readers in plant stress response has been addressed previously (Liu et al., 2020; Lu et al., 2020: Sun et al., 2020; Manavski et al., 2021a; Shao et al., 2021; Qin et al.,

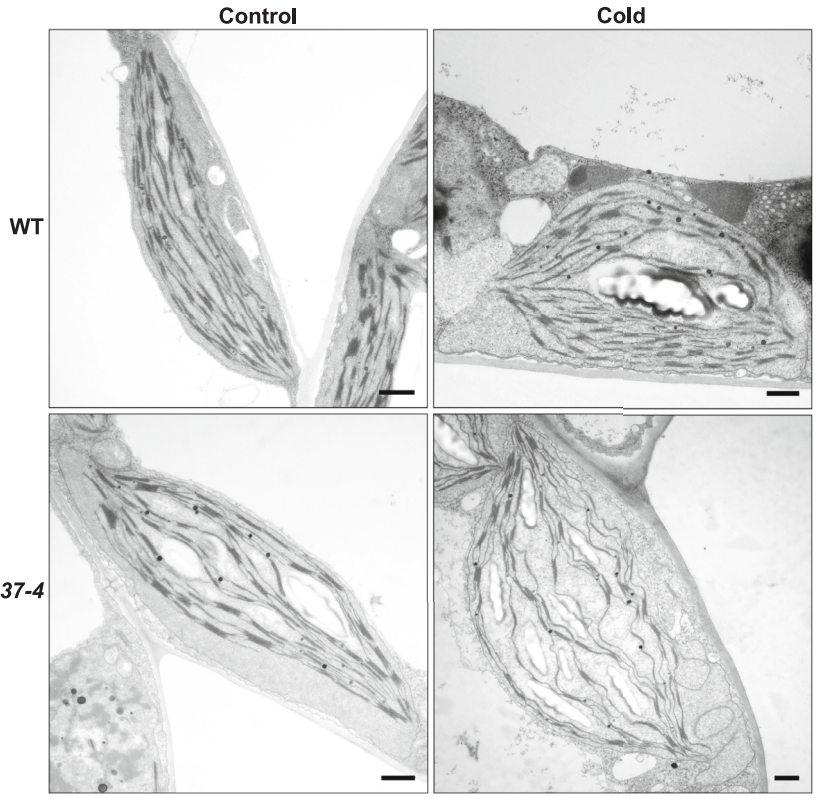

Figure 6. Chloroplast ultrastructure of WT and *fip37-4* grown under standard and cold conditions.
Representative transmission electron micrographs of WT and *fip37-4* chloroplasts. Plants were cultivated on Murashige and Skoog medium for 10 days under standard conditions and then placed in the cold for 4 days. Scale bar: 1 μm.

2022; Zhang et al., 2022). The results presented here demonstrate that expression of all 42 chloroplast-associated epitranscriptomic players studied was responsive to cold, heat, and high light acclimation. Reversibility of the expression changes upon deacclimation strongly suggests that these factors have important modulating roles under these particular conditions (Figure 1A). The expression signature of most relevant down- and upregulated epitranscriptomic factors after NF treatment could not be properly modified by *gun* mutants, indicating that GUN factors rarely interfere with retrograde communication regarding RNA modifications (Figure 1B). Overall, these data provide evidence for the hierarchy of regulation of posttranscriptional RNA modification, in which the chloroplast plays a central role as an environmental sensor and trigger for mainly *gun*-independent retrograde signaling.

Consistent with upregulated gene expression of writer complex components in the cold, m^{6}A marks of cellular mRNAs also increased, indicating a reshaping of the cellular m^{6}A methylome during cold acclimation (Figures 1C–1E). The ability of the chloroplast itself to act on the cellular m^{6}A transcriptome through retrograde signals suggests an important link between the perception of external stimuli and the cellular m^{6}A methylome (Figure 1B). Here, we showed that FIP37, as a central subunit of the main nuclear m^{6}A writer complex, plays an important role in regulation of multifaceted and dynamic processes related to photosynthesis, chloroplast development, and chloroplast structure during cold treatment. Moreover, we observed that the cold sensitivity of *fip37-4*, in terms of Fv/Fm, was independent of age, size, and developmental stage.

Interestingly, the writer mutant *vir-1* has a clear and sudden effect on PSII accumulation after high light treatment (Zhang et al., 2022), whereas cold affects PSI in *fip37-4*. This reflects a rapid response to the generally faster occurrence of sudden high light compared with slower temperature decreases in nature and again suggests defined strategies of the cellular m^{6}A RNA methylome for coping with different stressors. The qualitatively and temporally distinct effects of cold and high light treatment on m^{6}A writer mutants also suggest that the activity and/or targets of the m^{6}A writer complex change according to environmental cues. Thus, the cellular m^{6}A methylome provides not only a regulatory platform but also an opportunity to interact with the multifaceted effects of cold and other stressors on plant processes, often primarily related to photosynthesis and chloroplast organization.

The fact that m^{6}A writer mutants showed essentially no marked effects on photosynthesis under standard conditions provides evidence for an important and distinct role of the cellular m^{6}A epitranscriptome in the cold and high light. Clearly, writer-induced m^{6}A marks and their effects on the fate of mRNAs that preferentially encode chloroplast proteins positively influence photosynthesis on multiple levels under unfavorable conditions.

Evidence for a beneficial impact of m^{6}A RNA methylation on plant performance under drought stress has only recently been described. When the methyltransferase MTB of watermelon was overexpressed in tobacco, transgenic plants showed increased drought tolerance and decreased photoinhibition, most likely due to enhanced scavenging of ROS species under drought (He et al., 2021). Furthermore, when apple plants were exposed to drought, expression of the methyltransferase *MdMTA* and m^{6}A levels were both induced to promote stability and translation efficiency of transcripts involved in lignin deposition and ROS scavenging (Hou et al., 2022).

The influence of methylation on photosynthesis is also supported by the fact that mRNAs associated with chloroplast functions are frequently methylated (Shen et al., 2016; Manavski et al., 2021a; Qin et al., 2022). Moreover, photosynthetic leaves have the highest extent of m^{6}A methylation among different organs (Wan et al., 2015). In addition, m^{6}A demethylases, such as ALKBH9B (*AT2G17970*) and ALKBH10B (*AT4G02940*), were downregulated in the cold (Figure 1A). Depending on the

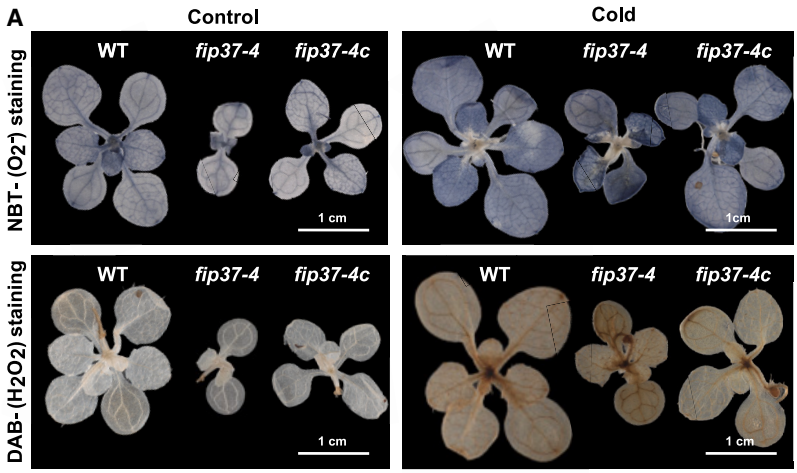

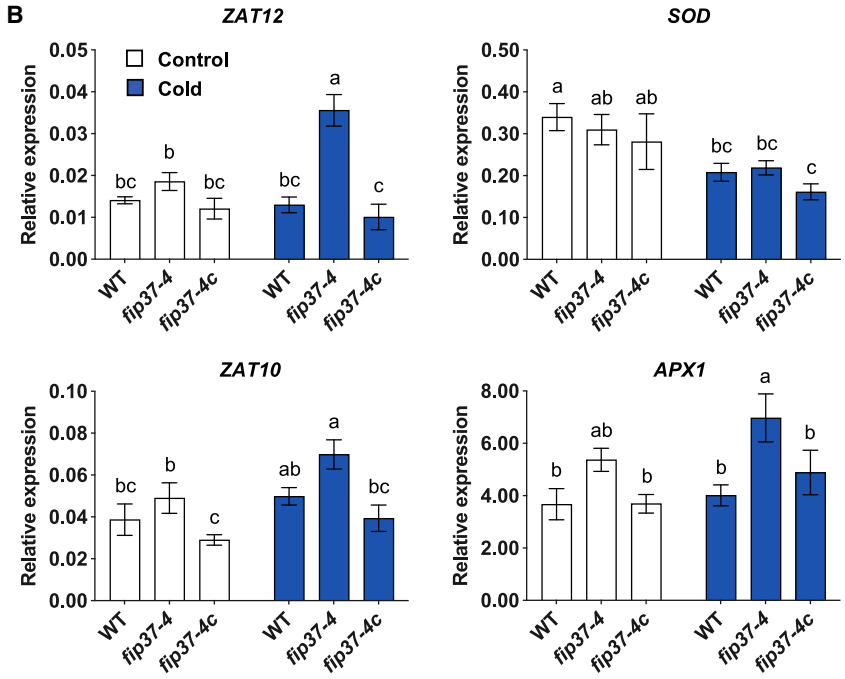

Figure 7. Cold treatment leads to increased accumulation of ROS in *fip37-4*.

(A) NBT and DAB staining of plants before or after 4 days of cold treatment. NBT staining is indicative of superoxide (O_2^-) production and DAB staining of H_2O_2 production. Scale bar: 1 cm.

(B) Expression of ROS-related genes (*ZAT12*, *ZAT10*, *SOD1*, and *APX1*) analyzed by qRT–PCR. Bars denote the means of 3 independent biological replicates with the corresponding standard deviations. Different letters within individual titles represent significant differences between tested temperatures (22°C and 4°C) and genotypes (WT, *fip37-4*, and *fip37-4c*) according to two-way ANOVA with post hoc Tukey's HSD ($p \leq 0.05$).

stressor, epitranscriptomic players can be either up- or downregulated. For instance, expression of the RNA demethylase ALKBH6 increased under salt stress (NaCl) but decreased under cold (Huong et al., 2020). Interestingly, *alkbh6* mutants grew more slowly and had a lower survival rate at high temperature compared with the WT (Huong et al., 2020). These results are consistent with our expression analysis of m^{6}A erasers and confirm the downregulation of other *Arabidopsis* m^{6}A demethylases at low temperatures (Figure 1A). Together, these results strongly suggest that m^{6}A players may have specific roles under distinct environmental conditions.

S-adenosylmethionine synthetase (SAMS) is an enzyme that uses ATP and methionine to catalyze the biosynthesis of S-adenosylmethionine, the substrate for methylation of numerous secondary metabolites and macromolecules as well as DNA and RNA writer enzymes. Interestingly, SAMS is known to confer resistance to drought, cold, and oxidative stress in overexpression lines (He et al., 2019; Choi et al., 2022). Both the enzymatic activity and gene expression of SAMS increased in the cold compared with control conditions, showing a correlation with expression of the m^{6}A writer components (Figures 1B and 1C). Under drought, oxidative stress, and low temperatures, SAMS-overexpressing *Nicotiana benthamiana* lines displayed lower ion leakage than the WT, suggesting that SAMS proteins are important for stress resistance (Choi et al., 2022). However, no correlations with methylation of RNAs or other molecules or photosynthesis were evaluated, and this would be an interesting task for future research.

Photosynthetic parameters were consistent with downregulation of proteins of PSI, the Cytb_6f complex, and the CET in *fip37-4* in the cold (Figures 2, 3, 4, and 5 and Supplemental Figure 4). However, slight changes in the levels of cytoplasmic and plastid transcripts of PSI, PSII, and Cytb_6f in the mutant did not correlate with protein amounts (Figures 4 and 5). This implies that m^{6}A-mediated posttranscriptional processes, such as export of RNA from the nucleus, translation, and/or protein stability, account for the cold sensitivity of the mutant. Protein deficiencies in cold-treated *fip37-4* mutants compared with the WT were consistent with accumulation of cytosolic monosomes (Figure 5B). Indeed, *in vivo* labeling experiments clearly showed a general decrease in translation efficiency in the cytosol of cold-treated *fip37-4* (Figure 5B). This demonstrates the mechanism by which FIP37 acts on cytoplasmic RNAs that mainly encode chloroplast proteins, including *rbcS*, and thus explains the reduced levels of chloroplast proteins. Polysome-seq analysis recently confirmed that the translation efficiency of approximately one-third of the genes in the *Arabidopsis* genome was dysregulated in response to cold in hypomorphic mutants of the writer complex (Wang et al., 2023). Given that cytoplasmic transcripts encoding chloroplast proteins were highly enriched in m^{6}A marks compared with transcripts with other functions, translational defects in these transcripts in

m^{6}A writer mutants primarily affected chloroplasts in the cold (Figure 5).

Reduced biomass production, retarded growth of primary roots, and accumulation of ROS during cold treatment were recently described in the *Arabidopsis mta* mutant (Govindan et al., 2022). Root length was not significantly altered when *fip37-4* was grown at 22°C for 3 weeks (Supplemental Figures 7A–7C). However, when plants were cultured at 4°C for a longer period, the root length of the mutant was, on average, about 4 times shorter than that of the WT, and growth was retarded in the mutant (Supplemental Figures 7A–7C). This hypersensitivity to cold could well be explained by the deleterious effect of the mutations on photosynthesis and other chloroplast functions described here. The unaltered ability of the mutant to induce expression of genes required for cold response and ROS scavenging shows that FIP37 is not required for this induction at the level of RNA accumulation.

CURT1 protein levels were also downregulated, and thylakoid curvature was altered accordingly in *fip37-4* in the cold. The nuclear-encoded CURT1 proteins are chloroplast localized (Armbruster et al., 2013), and the number of m^{6}A sites in RNAs of CurT1A–CurtT1D vary between the WT and *fip37-4* (Qin et al., 2022). Therefore, m^{6}A marks also seem to have important functions in the organization of the thylakoid membrane (Figure 6).

Regardless of the genetic compartment, RNA methylation can strongly influence chloroplast functions and stabilize photosynthesis under unfavorable environmental conditions. All these findings characterized cellular m^{6}A-methylation marks as a central, dynamic, and complex platform that governs gene expression in all plant genetic compartments. They also established a link between m^{6}A RNA methylation and chloroplast functions that enables plants to respond positively to cold and other challenging conditions at multiple levels.

METHODS

Plant materials and growth conditions

We used the *Arabidopsis thaliana* accession Col-0 as the WT control and the previously described *HAKAI* knockout and knockdown lines for *FIP37* (*fip37-4*), *MTA* (*mta*), *VIRILIZER* (*vir-1*), and the corresponding complemented lines *vir-1c* and *fip37-4c* (Shen et al., 2016; Růžička et al., 2017; Parker et al., 2020). Plants were cultivated on half-strength Murashige and Skoog medium supplemented with 1.5% sucrose or on soil under long-day standard conditions (16 h at 22°C and 80 μmol photons m^{-2} s^{-1}/8 h at 18°C in the dark) using light-emitting diode cabinets (LED-41 HIL2, Percival Scientific, Perry, IA, USA). Surface-sterilized seeds were stratified at 4°C for 2 days and then cultivated for 10–21 days under standard conditions. For high light acclimation, the light intensity was increased to 450 μmol photons m^{-2} s^{-1}. For cold and heat treatments, plants were grown at constant temperatures of 4°C and 32°C, respectively. Acclimation treatments were applied after standard growth conditions for up to 4 days. To test deacclimation, plants were transferred to standard conditions for 4 additional days after heat, cold, and high light treatments.

Transcript analysis

Transcriptome data were retrieved from Garcia-Molina et al. (2020) and Koussevitzky et al. (2007) (GEO: GSE125950 and GSE12887, respectively). Heatmaps were elaborated with the package *pheatmap* integrated in RStudio (https://www.bioconductor.org). Gene expression analyses using 10-day-old seedlings, total RNA isolation, electrophoresis, gel blotting, and hybridization with radioactive [^{32}P]-dCTP-labeled probes were performed as described previously (Manavski et al., 2015). Primers for PCR probes and oligonucleotides are listed in Supplemental Table 2.

Protein analysis

Immunoblot analyses were performed with total proteins isolated from WT and *fip37-4* seedlings in extraction buffer (100 mM NaCl, 50 mM Tris–HCl [pH 7.5], 0.5% [v/v] Triton X-100, 1 mM DTT) as described previously (Schmid et al., 2019). Equal amounts of total protein (10 μg) were loaded onto 10% polyacrylamide (w/v) Mini-PROTEAN SDS-PAGE gels (Bio-Rad); fractionated by electrophoresis and blotted onto PVDF membranes; blocked with 5% (w/v) milk powder prepared in TBS-T (50 mM Tris–HCl [pH 7.5], 150 mM NaCl, 0.1% [v/v] Tween 20); and incubated overnight with primary antibodies specific for PsaA, PsaD, PsaO, D1, D2, PsbO, LHCB6, Cytb_6, Cyt*f*, AtpB, NdhB (Agrisera, https://www.agrisera.com), PGR5 (Munekage et al., 2002), and CurT1 (Armbruster et al., 2013). After subsequent washing steps, membranes were incubated with the appropriate peroxidase-conjugated secondary antibody. Immunoblots were developed with the SuperSignal West Pico PLUS Chemiluminescent Substrate (Thermo Scientific) using the Fusion FX7 GelDoc (PeqLab).

In vivo labeling was essentially performed as described previously (Manavski et al., 2021b), except that instead of leaf discs, 4-day-old cold-treated seedlings were used. Prior to incubation with [^{35}S] methionine at a final concentration of 50 mCi (specific activity >1000 Ci/mmol), seedlings were incubated for 30 min in the dark in labeling buffer supplemented with either 250 μg/ml chloramphenicol or 50 μg/ml cycloheximide. Labeled proteins were blotted onto a PVDF membrane and visualized by phosphorimaging (Amersham, Typhoon laser scanner).

Blue native PAGE

Isolation and solubilization of thylakoids were performed as described previously (Meurer et al., 2017). Proteins normalized to chlorophyll content were loaded onto a NativePAGE 3%–12%, Bis-Tris, 1 mm, Mini Protein Gel (Thermo Scientific) and separated at 200 V in the cold. Proteins were then either transferred onto PVDF membranes or stained with ROTIBlue quick (Roth).

Preparation of nucleosides for m^{6}A quantification using LC–MS

For LC–MS, total RNA was extracted from 10-day-old WT seedlings before and after 4 days of cold, heat, or high light treatment. DNase treatment was performed using 10 μg total RNA (Zymo, RNA isolation kit). For poly(A)-enriched mRNAs, the NEBNext Poly(A) mRNA Magnetic Isolation kit (New England Biolabs) was used, and RNA integrity was confirmed with a Bioanalyzer (Agilent RNA 6000 Pico). RNAs were then concentrated in a speed vacuum centrifuge (Eppendorf Concentrator 5301) and precipitated overnight using 5 μl 5 M ammonium acetate and 125 μl cold 100% ethanol. Prior to LC–MS, samples were centrifuged for 1 h at 4°C, and the pellets were resuspended in RNase-free water. RNA was digested to single nucleosides using 2 U alkaline phosphatase, 0.2 U phosphodiesterase I (VWR, Radnor, PA, USA), 2 U benzonase in 5 mM Tris buffer (pH 8), and 1 mM $MgCl_2$. Furthermore, 0.5 μg tetrahydrouridine (Merck, Darmstadt, Germany), 1 μM butylated hydroxytoluene, and 0.1 μg pentostatin were added in order to avoid deamination and oxidation of the nucleosides. After incubation for 2 h at 37°C, 10 μl LC–MS buffer (5 mM NH_4OAc [pH 5.3]) was added, and LC–MS was performed.

LC–MS of hydrolyzed nucleosides

LC–MS experiments were performed on an Agilent 1290 Infinity II equipped with a Phenomenex Synergi 2.5 μm Fusion-RP 100 Å column

(100 × 2 mm) coupled to an Agilent 6470 Triple Quad equipped with an ESI ion source. Ten microliters of each sample were injected without prior filtering. Chromatographic separation was carried out at 35°C with a flow rate of 0.35 ml/min using a linear gradient of two solvents: 5 mM ammonium acetate (pH 5.3) as solvent A and acetonitrile as solvent B (gradient: 0–1 min kept at 0% B, 1–5 min increase to 10% B, 5–7 min increase to 40% B, 7–8 min kept at 40% B, 8–8.5 min decrease to 0% B, 8.5–11 min kept at 0% B). Quantification was performed using calibration curves of synthetic standards and stable isotope-labeled internal standards (20 ng in 1 μl was automatically added by the instrument per sample) for each nucleoside (Heiss et al., 2021) using Agilent MassHunter software (v.9.0.647.0). To obtain the calibration curves, a solution containing synthetic standards of all nucleosides was serially diluted by a factor of 1:2 (12 calibration levels). The highest injected amounts were 100 (C, U, G, A) or 5 pmol (m^{6}A).

Photosynthetic measurements

Photosynthetic measurements were performed on seedlings using an IMAGING or DUAL PAM instrument (Heinz Walz), essentially as previously described (Lezhneva and Meurer 2004). Dark-adapted leaves were used to determine the maximum quantum yield of PSII (Fv/Fm). Φ(II), Φ(NPQ), and Φ(NO) were calculated at steady state with leaves adapted to actinic light intensities of 80 μmol photons m^{-2} s^{-1}. Saturating light pulses with a duration of 800 ms and a light intensity of 6000 μmol photons m^{-2} s^{-1} were used. The quantum yield of PSI Φ(I), as well as acceptor Φ(NA) and donor side Φ(ND) limitations, were measured as described previously (Plöchinger et al., 2016).

Transmission electron microscopy

For transmission electron microscopy, 10-day-old seedlings of WT and *fip37-4* cultivated on Murashige and Skoog medium supplemented with sucrose were analyzed before and after 4 days of cold treatment. Plants were stored in the dark for 16 h before fixation to avoid starch accumulation. Primary leaves were cut into 1-mm^2 pieces and fixed for 1–3 days at 4°C in cacodylate buffer (75 mM sodium cacodylate, 2 mM $MgCl_2$ [pH 7], supplemented with 2.5% glutaraldehyde) as described previously (Garcia-Molina et al., 2020). After postfixation with 1% (w/v) OsO_4 for 1 h, *en bloc* staining with 1% (w/v) uranyl acetate in 20% (v/v) acetone and dehydration in a graded acetone series were performed, and the plant material was embedded in Spurr's resin. Ultrathin sections were contrasted with lead citrate and examined with a Zeiss EM 912 transmission electron microscope (Zeiss, Oberkochen, Germany) operating at 80 kV in the zero-loss mode. Images were acquired with a Tröndle 2k × 2k slow-scan CCD camera (TRS, Moorenweis, Germany). Images were processed with FIJI v.2.1 (https://fiji.sc).

ROS measurements

In situ detection of superoxide and H_2O_2 was performed with NBT and DAB, respectively, as described previously (Fryer et al., 2002; Wohlgemuth et al., 2002). In brief, *Arabidopsis* plants were vacuum infiltrated with 0.1% NBT, 50 mM potassium phosphate buffer (pH 7.8), and 10 mM sodium azide for 20 min, then incubated for 1 h at room temperature. Plants were then boiled in 95% ethanol for 15 min to remove chlorophyll. For H_2O_2 detection, plants were vacuum infiltrated with 5 mM DAB–HCl (pH 3) for 20 min and incubated in the same solution for at least 8 h overnight. Plants were then boiled in ethanol:acetic acid:glycerol (3:1:1) solution under the hood until they turned transparent and were later photographed.

qRT–PCR

For qRT–PCR, rosettes of at least five plants grown *in vitro* were harvested and homogenized in liquid nitrogen. RNA extraction was performed with the NucleoSpin RNA Plant Kit (Macherey-Nagel, Düren, Germany) according to the manufacturer's protocol. RNA purity and concentration were determined using a NanoDrop spectrophotometer. Total RNA was transcribed into cDNA using the qScript cDNA Synthesis Kit (Quantabio, Beverly, MA, USA). The qPCR was performed in 10 μl using the Quantabio SYBR Green quantification kit on the PFX96 system (BioRad, Hercules, CA, USA) with the specific primers listed in Supplemental Table 2. After 3 min of denaturation at 95°C, 39 cycles were performed (95°C 10 s, 60°C 40 s). Actin (*At2g37620*) was used as a reference for transcript normalization. The expression of each gene was calculated in relation to the reference. The relative transcript levels of the different genes were evaluated by scoring the runs according to the following formula: copy number = $E(\text{reference})^{CT}/E(\text{GOI})^{CT}$ (E, primer efficiency factor; CT, number of cycles; GOI, gene of interest) essentially as described previously (Vandesompele et al., 2002). Mean values and standard deviations were calculated from at least three biological replicates in technical duplicates.

RNA gel blot and polysome loading analysis

RNA gel blots were prepared as described previously (Stoppel et al., 2011). Nylon membranes were hybridized overnight with either radioactively labeled PCR products or 80-mer probes at 65°C or 55°C, respectively, as described previously (Manavski et al., 2015). Sequences of the primers and 80-mers are listed in Supplemental Table 2. Polysome loading analysis was performed essentially as described previously (Meurer et al., 2002).

Chlorophyll and anthocyanin measurements

Chlorophyll measurements were performed as described previously (Porra and Scheer, 2019). Anthocyanin content was calculated by measuring the absorption of the aqueous phase at 530 and 657 nm (Neff and Chory, 1998).

ACCESSION NUMBERS

Sequence data from this article can be found in the GenBank/EMBL data libraries under locus numbers *AT3G54170* (*FIP37*), *AT5G01160* (*HAKAI*), *AT3G05680* (*VIR*), *AT4G10760* (*MTA*), and *AT4G09980* (*MTB*).

SUPPLEMENTAL INFORMATION

Supplemental information is available at *Plant Communications Online*.

FUNDING

This research was supported by the Deutsche Akademischer Austauschdienst (91692277 to A.M.V.) and the Deutsche Forschungsgemeinschaft (TRR 175 projects B07 to D.L., B08 to T.M., and A03 to J.M.).

AUTHOR CONTRIBUTIONS

A.M.V., N.M., L.-M.S., P.T.R., C.S., L.B., G.A., A.G.-M., and J.M. performed the research. A.M.V., N.M., T.M., D.L., S.K., and J.M. analyzed the data. A.M.V. and J.M. designed the work and wrote the article with the contribution of all coauthors.

ACKNOWLEDGMENTS

We thank Gordon G. Simpson (University of Dundee) for kindly providing *fip37-4*, *vir-1*, and *vir-1c* lines, Hao Yu (University of Singapore) for *fip37-4c* lines, and Rupert G. Fray (University of Nottingham) for *hakai* and *mta* seeds. We also thank Andreas Klingl for providing the electron microscopy facility. No conflict of interest is declared.

Received: February 8, 2023
Revised: May 10, 2023
Accepted: June 3, 2023
Published: June 7, 2023

REFERENCES

Anderson, S., Kramer, M., Gosai, S., Yu, X., Vandivier, L., Nelson, A., Anderson, Z., Beilstein, M., Fray, R., Lyons, E., et al. (2018). N^6-Methyladenosine inhibits local ribonucleolytic cleavage to stabilize mRNAs in arabidopsis. Cell Rep. **25**:1146–1157. https://doi.org/10.1016/j.celrep.2018.10.020.

Armbruster, U., Labs, M., Pribil, M., Viola, S., Xu, W., Scharfenberg, M., Hertle, A., Rojahn, U., Jensen, P., Rappaport, F., et al. (2013). Arabidopsis CURVATURE THYLAKOID1 proteins modify thylakoid architecture by inducing membrane curvature. Plant Cell **25**:2661–2678. https://doi.org/10.1105/tpc.113.113118.

Boccaletto, P., Machnicka, M.A., Purta, E., Piątkowski, P., Bagiński, B., Wirecki, T.K., de Crécy-Lagard, V., Ross, R., Limbach, P.A., Kotter, A., et al. (2021). Modomics: a database of RNA modification pathways. Nucleic Acids Research. **46**:303–307. https://doi.org/10.1093/nar/gkab1083.

Chinnusamy, V., Zhu, J., and Zhu, J.-K. (2007). Cold stress regulation of gene expression in plants. Trends Plant Sci. **12**:444–451. https://doi.org/10.1016/j.tplants.2007.07.002.

Choi, H.L., Seo, J.W., Hwang, M.H., Yu, C.Y., and Seong, E.S. (2022). A cold stress-responsive gene, provides resistance to environmental stress in T2-generation transgenic plants. Transgenic Res. **31**:381–389. https://doi.org/10.1007/s11248-022-00307-9.

Crawford, T., Lehotai, N., and Strand, Å. (2018). The role of retrograde signals during plant stress responses. J. Exp. Bot. **69**:2783–2795. https://doi.org/10.1093/jxb/erx481.

Crosatti, C., Rizza, F., Badeck, F.W., Mazzucotelli, E., and Cattivelli, L. (2013). Harden the chloroplast to protect the plant. Physiol. Plantarum **147**:55–63. https://doi.org/10.1111/j.1399-3054.2012.01689.x.

Fryer, M.J., Oxborough, K., Mullineaux, P.M., and Baker, N.R. (2002). Imaging of photo-oxidative stress responses in leaves. J. Exp. Bot. **53**:1249–1254. https://doi.org/10.1093/jexbot/53.372.1249.

Garcia-Molina, A., Kleine, T., Schneider, K., Mühlhaus, T., Lehmann, M., and Leister, D. (2020). Translational components contribute to acclimation responses to high light, heat, and cold in arabidopsis. iScience **23**:101331. https://doi.org/10.1016/j.isci.2020.101331.

Govindan, G., Sharma, B., Li, Y.F., Armstrong, C.D., Merum, P., Rohila, J.S., Gregory, B.D., and Sunkar, R. (2022). mRNA N^6-methyladenosine is critical for cold tolerance in Arabidopsis. Plant J. **111**:1052–1068. https://doi.org/10.1111/tpj.15872.

He, M.-W., Wang, Y., Wu, J.-Q., Shu, S., Sun, J., and Guo, S.-R. (2019). Isolation and characterization of S-Adenosylmethionine synthase gene from cucumber and responsive to abiotic stress. Plant Physiol. Biochem. **141**:431–445. https://doi.org/10.1016/j.plaphy.2019.06.006.

He, Y., Li, Y., Yao, Y., Zhang, H., Wang, Y., Gao, J., and Fan, M. (2021). Overexpression of watermelon m^{6}A methyltransferase ClMTB enhances drought tolerance in tobacco by mitigating oxidative stress and photosynthesis inhibition and modulating stress-responsive gene expression. Plant Physiol. Biochem. **168**:340–352. https://doi.org/10.1016/j.plaphy.2021.10.007.

Heiss, M., Borland, K., Yoluç, Y., and Kellner, S. (2021). Quantification of modified nucleosides in the context of NAIL-MS. Methods Mol. Biol. **2298**:279–306. https://doi.org/10.1007/978-1-0716-1374-0_18.

Hou, N., Li, C., He, J., Liu, Y., Yu, S., Malnoy, M., Mobeen Tahir, M., Xu, L., Ma, F., and Guan, Q. (2022). MdMTA-mediated m^{6}A modification enhances drought tolerance by promoting mRNA stability and translation efficiency of genes involved in lignin deposition and oxidative stress. New Phytol. **234**:1294–1314. https://doi.org/10.1111/nph.18069.

Hu, J., Cai, J., Park, S.J., Lee, K., Li, Y., Chen, Y., Yun, J.-Y., Xu, T., and Kang, H. (2021). N^6-Methyladenosine mRNA methylation is important for salt stress tolerance in Arabidopsis. Plant J. **106**:1759–1775. https://doi.org/10.1111/tpj.15270.

Huong, T.T., Ngoc, L.N.T., and Kang, H. (2020). Functional characterization of a putative RNA demethylase ALKBH6 in arabidopsis growth and abiotic stress responses. Int. J. Mol. Sci. **21**:6707. https://doi.org/10.3390/ijms21186707.

Kleine, T., Nägele, T., Neuhaus, H.E., Schmitz-Linneweber, C., Fernie, A.R., Geigenberger, P., Grimm, B., Kaufmann, K., Klipp, E., Meurer, J., et al. (2021). Acclimation in plants - the green hub consortium. Plant J. **106**:23–40. https://doi.org/10.1111/tpj.15144.

Koussevitzky, S., Nott, A., Mockler, T.C., Hong, F., Sachetto-Martins, G., Surpin, M., Lim, J., Mittler, R., and Chory, J. (2007). Signals from chloroplasts converge to regulate nuclear gene expression. Science **316**:715–719. https://doi.org/10.1126/science.1114655.

Lezhneva, L., and Meurer, J. (2004). The nuclear factor HCF145 affects chloroplast *psaA-psaB-rps14* transcript abundance in *Arabidopsis thaliana*. Plant J. **38**:740–753. https://doi.org/10.1111/j.1365-313X.2004.02081.x.

Li, M., and Kim, C. (2022). Chloroplast ROS and stress signaling. Plant Commun. **3**:100264. https://doi.org/10.1016/j.xplc.2021.100264.

Li, J.-Y., Yang, C., Tian, Y.-Y., and Liu, J.-X. (2022). Regulation of chloroplast development and function at adverse temperatures in plants. Plant Cell Physiol. **63**:580–591. https://doi.org/10.1093/pcp/pcac022.

Liang, Z., Riaz, A., Chachar, S., Ding, Y., Du, H., and Gu, X. (2020). Epigenetic modifications of mRNA and DNA in plants. Mol. Plant **13**:14–30. https://doi.org/10.1016/j.molp.2019.12.007.

Liu, Y., Dang, P., Liu, L., and He, C. (2019). Cold acclimation by the CBF-COR pathway in a changing climate: lessons from. Plant Cell Rep. **38**:511–519. https://doi.org/10.1007/s00299-019-02376-3.

Liu, G., Wang, J., and Hou, X. (2020). Transcriptome-wide N^6-methyladenosine (m^{6}A) methylome profiling of heat stress in pak-choi (*Brassica rapa ssp. chinensis*). Plants **9**:1080. https://doi.org/10.3390/plants9091080.

Lu, L., Zhang, Y., He, Q., Qi, Z., Zhang, G., Xu, W., Yi, T., Wu, G., and Li, R. (2020). MTA, an RNA m^{6}A methyltransferase, enhances drought tolerance by regulating the development of trichomes and roots in poplar. Int. J. Mol. Sci. **21**:2462. https://doi.org/10.3390/ijms21072462.

Luo, G.Z., MacQueen, A., Zheng, G., Duan, H., Dore, L.C., Lu, Z., Liu, J., Chen, K., Jia, G., Bergelson, J., et al. (2014). Unique features of the m^{6}A methylome in Arabidopsis thaliana. Nat. Commun. **5**:5630–5638. https://doi.org/10.1038/ncomms6630.

Manavski, N., Torabi, S., Lezhneva, L., Arif, M.A., Frank, W., and Meurer, J. (2015). HIGH CHLOROPHYLL FLUORESCENCE145 binds to and stabilizes the *psaA* 5'UTR via a newly defined repeat motif in embryophyta. Plant Cell **27**:2600–2615. https://doi.org/10.1105/tpc.15.00234.

Manavski, N., Schmid, L.M., and Meurer, J. (2018). RNA-stabilization factors in chloroplasts of vascular plants. Essays Biochem. **62**:51–64. https://doi.org/10.1042/EBC20170061.

Manavski, N., Vicente, A., Chi, W., and Meurer, J. (2021a). The chloroplast epitranscriptome: factors, sites, regulation, and detection methods. Genes **12**:1121–1122. https://doi.org/10.1042/EBC20170061.

Manavski, N., Mathieu, S., Rojas, M., Méteignier, L.V., Brachmann, A., Barkan, A., and Hammani, K. (2021b). In vivo stabilization of endogenous chloroplast RNAs by customized artificial pentatricopeptide repeat proteins. Nucleic Acids Res. **49**:5985–5997. https://doi.org/10.1093/nar/gkab390.

Meurer, J., Meierhoff, K., and Westhoff, P. (1996). Isolation of *high-chlorophyll-fluorescence* mutants of *Arabidopsis thaliana* and their characterization by spectroscopy, immunoblotting and northern hybridisation. Planta **198**:385–396. https://doi.org/10.1007/BF00620055.

Meurer, J., Lezhneva, L., Amann, K., Gödel, M., Bezhani, S., Sherameti, I., and Oelmüller, R. (2002). A peptide chain release factor 2 affects the stability of UGA-containing transcripts in Arabidopsis chloroplasts. Plant Cell **14**:3255–3269. https://doi.org/10.1105/tpc.006809.

Meurer, J., Schmid, L.M., Stoppel, R., Leister, D., Brachmann, A., and Manavski, N. (2017). PALE CRESS binds to plastid RNAs and facilitates the biogenesis of the 50S ribosomal subunit. Plant J. **92**:400–413. https://doi.org/10.1111/tpj.13662.

Munekage, Y., Hojo, M., Meurer, J., Endo, T., Tasaka, M., and Shikanai, T. (2002). PGR5 is involved in cyclic electron flow around photosystem I and is essential for photoprotection in Arabidopsis. Cell **110**:361–371. https://doi.org/10.1016/s0092-8674(02)00867-x.

Nakaminami, K., and Seki, M. (2018). RNA regulation in plant cold stress response. Adv. Exp. Med. Biol. **1081**:23–44. https://doi.org/10.1007/978-981-13-1244-1_2.

Neff, M.M., and Chory, J. (1998). Genetic interactions between phytochrome A, phytochrome B, and cryptochrome 1 during Arabidopsis development. Plant Physiol. **118**:27–35. https://doi.org/10.1104/pp.118.1.27.

Parker, M.T., Knop, K., Sherwood, A.V., Schurch, N.J., Mackinnon, K., Gould, P.D., Hall, A.J., Barton, G.J., and Simpson, G.G. (2020). Nanopore direct RNA sequencing maps the complexity of Arabidopsis mRNA processing and m^{6}A modification. Elife **9**:1496588-35. https://doi.org/10.7554/eLife.49658.

Plöchinger, M., Torabi, S., Rantala, M., Tikkanen, M., Suorsa, M., Jensen, P.-E., Aro, E.M., and Meurer, J. (2016). The low molecular weight protein Psal stabilizes the light-harvesting complex II docking site of photosystem I. Plant Physiol. **172**:450–463. https://doi.org/10.1104/pp.16.00647.

Porra, R.J., and Scheer, H. (2019). Towards a more accurate future for chlorophyll *a* and *b* determinations: the inaccuracies of Daniel Arnon's assay. Photosynth. Res. **140**:215–219. https://doi.org/10.1007/s11120-018-0579-8.

Qin, H., Ou, L., Gao, J., Chen, L., Wang, J.W., Hao, P., and Li, X. (2022). DENA: training an authentic neural network model using Nanopore sequencing data of Arabidopsis transcripts for detection and quantification of N^6-methyladenosine on RNA. Genome Biol. **23**, 25-23. https://doi.org/10.1186/s13059-021-02598-3.

Richter, A.S., Tohge, T., Fernie, A.R., and Grimm, B. (2020). The genomes uncoupled-dependent signalling pathway coordinates plastid biogenesis with the synthesis of anthocyanins. Philos. Trans. R. Soc. Lond. B Biol. Sci. **375**:20190403. https://doi.org/10.1098/rstb.2019.0403.

Araguirang, G.E., and Richter, A.S. (2022). Activation of anthocyanin biosynthesis in high light - what is the initial signal? New Phytol. **236**:2037–2043. https://doi.org/10.1111/nph.18488.

Růžička, K., Zhang, M., Campilho, A., Bodi, Z., Kashif, M., Saleh, M., Eeckhout, D., El-Showk, S., Li, H., Zhong, S., et al. (2017). Identification of factors required for m^{6}A mRNA methylation in Arabidopsis reveals a role for the conserved E3 ubiquitin ligase HAKAI. New Phytol. **215**:157–172. https://doi.org/10.1111/nph.14586.

Schmid, L.M., Ohler, L., Möhlmann, T., Brachmann, A., Muiño, J.M., Leister, D., Meurer, J., and Manavski, N. (2019). PUMPKIN, the sole plastid UMP kinase, associates with group II introns and alters their metabolism. Plant Physiol. **179**:248–264. https://doi.org/10.1104/pp.18.00687.

Schwenkert, S., Fernie, A.R., Geigenberger, P., Leister, D., Möhlmann, T., Naranjo, B., and Neuhaus, H.E. (2022). Chloroplasts are key players to cope with light and temperature stress. Trends Plant Sci. **27**:577–587. https://doi.org/10.1016/j.tplants.2021.12.004.

Scutenaire, J., Deragon, J.M., Jean, V., Benhamed, M., Raynaud, C., Favory, J.J., Merret, R., and Bousquet-Antonelli, C. (2018). The YTH domain protein ECT2 is an m^{6}A reader required for normal trichome branching in Arabidopsis. Plant Cell **30**:986–1005. https://doi.org/10.1105/tpc.17.00854.

Shao, Y., Wong, C.E., Shen, L., and Yu, H. (2021). N^6-methyladenosine modification underlies messenger RNA metabolism and plant development. Curr. Opin. Plant Biol. **63**:102047. https://doi.org/10.1016/j.pbi.2021.102047.

Shen, L., Liang, Z., Gu, X., Chen, Y., Teo, Z.W.N., Hou, X., Cai, W.M., Dedon, P.C., Liu, L., and Yu, H. (2016). N^6-Methyladenosine RNA modification regulates shoot stem cell fate in arabidopsis. Dev. Cell **38**:186–200. https://doi.org/10.1016/j.devcel.2016.06.008.

Shen, L. (2023). Functional interdependence of N6-methyladenosine methyltransferase complex subunits in Arabidopsis. Plant Cell **35**:1901–1916. https://doi.org/10.1093/plcell/koad070.

Shi, H., Chai, P., Jia, R., and Fan, X. (2020). Novel insight into the regulatory roles of diverse RNA modifications: Re-defining the bridge between transcription and translation. Mol. Cancer **19**:78. https://doi.org/10.1186/s12943-020-01194-6.

Stoppel, R., Lezhneva, L., Schwenkert, S., Torabi, S., Felder, S., Meierhoff, K., Westhoff, P., and Meurer, J. (2011). Recruitment of a ribosomal release factor for light- and stress-dependent regulation of *petB* transcript stability in Arabidopsis chloroplasts. Plant Cell **23**:2680–2695. https://doi.org/10.1105/tpc.111.085324.

Sun, J., Bie, X.M., Wang, N., Zhang, X.S., and Gao, X.-Q. (2020). Genome-wide identification and expression analysis of YTH domain-containing RNA-binding protein family in common wheat. BMC Plant Biol. **20**:351. https://doi.org/10.1186/s12870-020-02505-1.

Theocharis, A., Clément, C., and Barka, E.A. (2012). Physiological and molecular changes in plants grown at low temperatures. Planta **235**:1091–1105. https://doi.org/10.1007/s00425-012-1641-y.

Vandesompele, J., De Preter, K., Pattyn, F., Poppe, B., Van Roy, N., De Paepe, A., and Speleman, F. (2002). Accurate normalization of real-time quantitative RT-PCR data by geometric averaging of multiple internal control genes. Genome Biol. **3**, RESEARCH0034. https://doi.org/10.1186/gb-2002-3-7-research0034.

Wan, Y., Tang, K., Zhang, D., Xie, S., Zhu, X., Wang, Z., and Lang, Z. (2015). Transcriptome-wide high-throughput deep m^{6}A-seq reveals unique differential m^{6}A methylation patterns between three organs in *Arabidopsis thaliana*. Genome Biol. **16**:272. https://doi.org/10.1186/s13059-015-0839-2.

Wang, Z., Tang, K., Zhang, D., Wan, Y., Wen, Y., Lu, Q., and Wang, L. (2017). High-throughput m^{6}A-seq reveals RNA m^{6}A methylation patterns in the chloroplast and mitochondria transcriptomes of *Arabidopsis thaliana*. PLoS One **12**:e0185612. https://doi.org/10.1371/journal.pone.0185612.

Wang, L., Zhuang, H., Fan, W., Zhang, X., Dong, H., Yang, H., and Cho, J. (2022). m^{6}A RNA methylation impairs gene expression variability and reproductive thermotolerance in Arabidopsis. Genome Biol. **23**:244. https://doi.org/10.1186/s13059-022-02814-8.

Wang, S., Wang, H., Xu, Z., Jiang, S., Shi, Y., Xie, H., Wang, S., Hua, J., and Wu, Y. (2023). m^{6}A mRNA modification promotes chilling tolerance and modulates gene translation efficiency in Arabidopsis. Plant Physiol. **192**:1466–1482. https://doi.org/10.1093/plphys/kiad112.

Winkel-Shirley, B. (2002). Biosynthesis of flavonoids and effects of stress. Curr. Opin. Plant Biol. **5**:218–223. https://doi.org/10.1016/s1369-5266(02)00256-x.

Wohlgemuth, H., Mittelstrass, K., Kschieschan, S., Bender, J., Weigel, H.-J., Overmyer, K., Kangasjärvi, J., Sandermann, H., and Langebartels, C. (2002). Activation of an oxidative burst is a general feature of sensitive plants exposed to the air pollutant ozone. Plant Cell Environ. **25**:717–726. https://doi.org/10.1046/j.1365-3040.2002.00859.x.

Wong, C.E., Zhang, S., Xu, T., Zhang, Y., Teo, Z.W.N., Yan, A., Shen, L., and Yu, H. (2023). Shaping the landscape of N6-methyladenosine RNA

methylation in Arabidopsis. Plant Physiol. **191**:2045–2063. https://doi.org/10.1093/plphys/kiad010.

Xu, Z., and Rothstein, S.J. (2018). ROS-Induced anthocyanin production provides feedback protection by scavenging ROS and maintaining photosynthetic capacity in Arabidopsis. Plant Signal. Behav. **13**:e1451708. https://doi.org/10.1080/15592324.2018.1451708.

Yu, X., Sharma, B., and Gregory, B.D. (2021). The impact of epitranscriptomic marks on posttranscriptional regulation in plants. Brief. Funct. Genomics **20**:113–124. https://doi.org/10.1093/bfgp/elaa021.

Zhang, M., Zeng, Y., Peng, R., Dong, J., Lan, Y., Duan, S., Chang, Z., Ren, J., Luo, G., Liu, B., et al. (2022). N^6-methyladenosine RNA modification regulates photosynthesis during photodamage in plants. Nat. Commun. **13**:7441. https://doi.org/10.1038/s41467-022-35146-z.

Plant Communications, Volume *4*

Supplemental information

The plant cytosolic m^{6}A RNA methylome stabilizes photosynthesis in the cold

Alexandre Magno Vicente, Nikolay Manavski, Paul Torben Rohn, Lisa-Marie Schmid, Antoni Garcia-Molina, Dario Leister, Charlotte Seydel, Leo Bellin, Torsten Möhlmann, Gregor Ammann, Stefanie Kaiser, and Jörg Meurer

Plant Communications

Supplemental information

The plant cytosolic m^{6}A RNA methylome stabilizes photosynthesis in the cold

Alexandre Magno Vicente, Nikolay Manavski, Paul Torben Rohn, Lisa-Marie Schmid, Antoni Garcia-Molina, Dario Leister, Charlotte Seydel, Leo Bellin, Torsten Möhlmann, Gregor Ammann, Stefanie Kaiser, Jörg Meurer

Supplemental Figures 1-7

Supplemental Tables 1-2

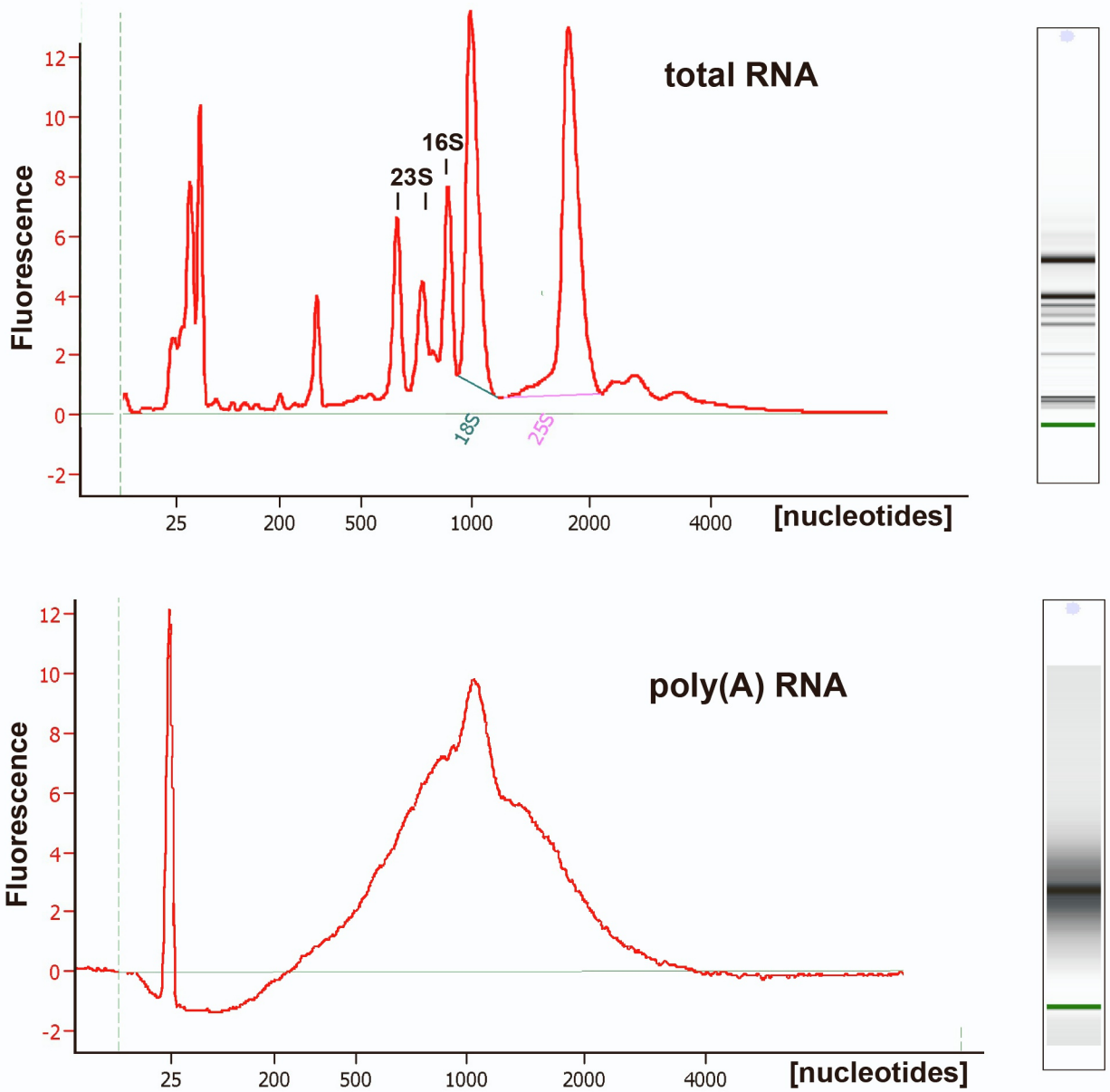

Supplemental Figure S1. Quality control of enriched poly(A)-RNA

Bioanalyzer electropherograms (RNA Pico 6.000) show representative samples of total (upper part) and poly(A)-enriched (lower part) RNAs used for m^6A quantification. Cellular rRNAs in total RNAs and their depletion in poly(A)-enriched RNA samples are shown. The presence of cytoplasmic 25S and 18S, and plastid 16S and 23S rRNA peaks indicated good integrity of RNAs. The corresponding virtual gels are shown on the right.

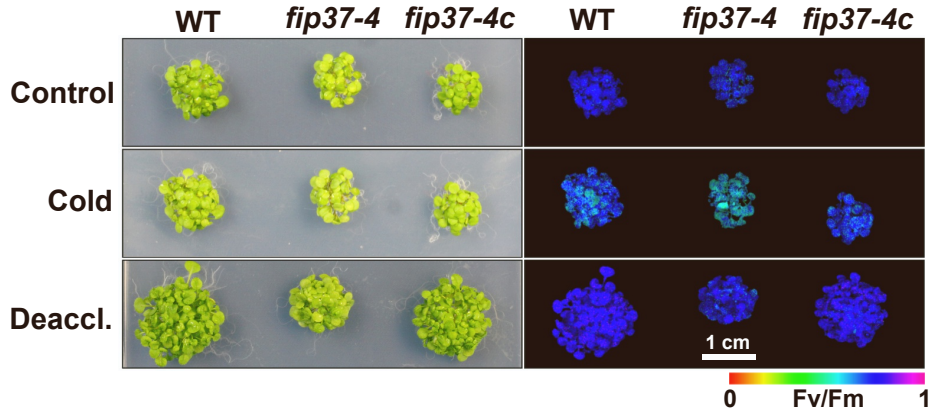

Supplemental Figure S2. FIP37 deficiency strongly but reversibly affects photosynthesis during cold treatment

The left part shows the visible phenotype of WT, *fip37-4,* and *fip37-4c* grown in vitro for 10 days under standard condition followed by 4 days in the cold and another 4 days of deacclimation. Corresponding chlorophyll fluorescence images reflecting Fv/Fm values are shown on the right. Scale bar: 1 cm.

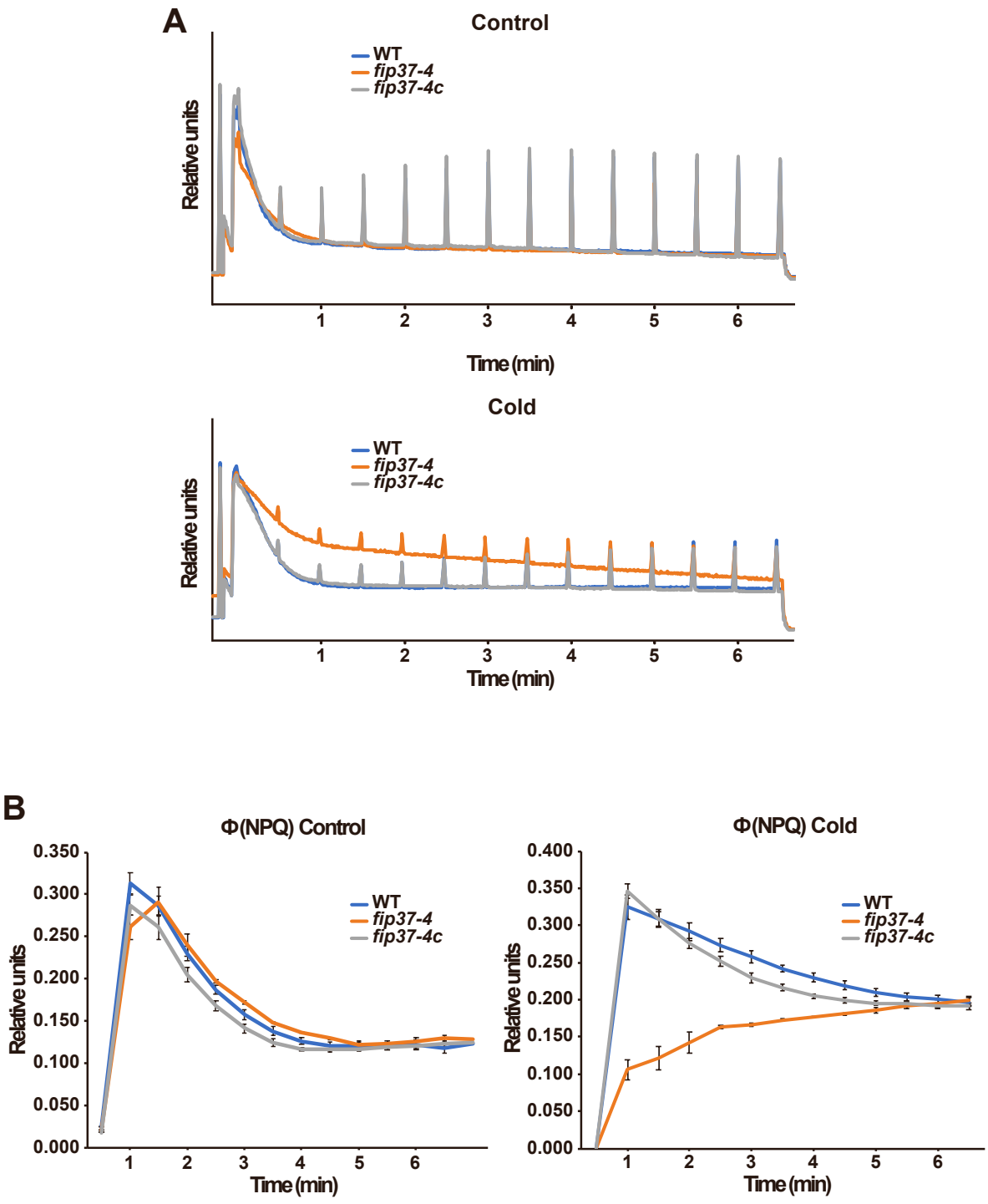

Supplemental Figure S3. Spectroscopic analysis of WT, *fip37-4,* and *fip37-4c*

(A) Representative chlorophyll fluorescence induction analysis of WT, *fip37-4,* and *fip37-4c* lines grown for 10 days under control and additional 4 days under cold conditions on soil. The actinic light intensity was set to 80 µmol photons m^{-2} s^{-1} and consecutive saturation pulses were applied every 30 s.

(B) The corresponding course of Φ(NPQ) during induction of plants grown under standard and cold conditions is shown.

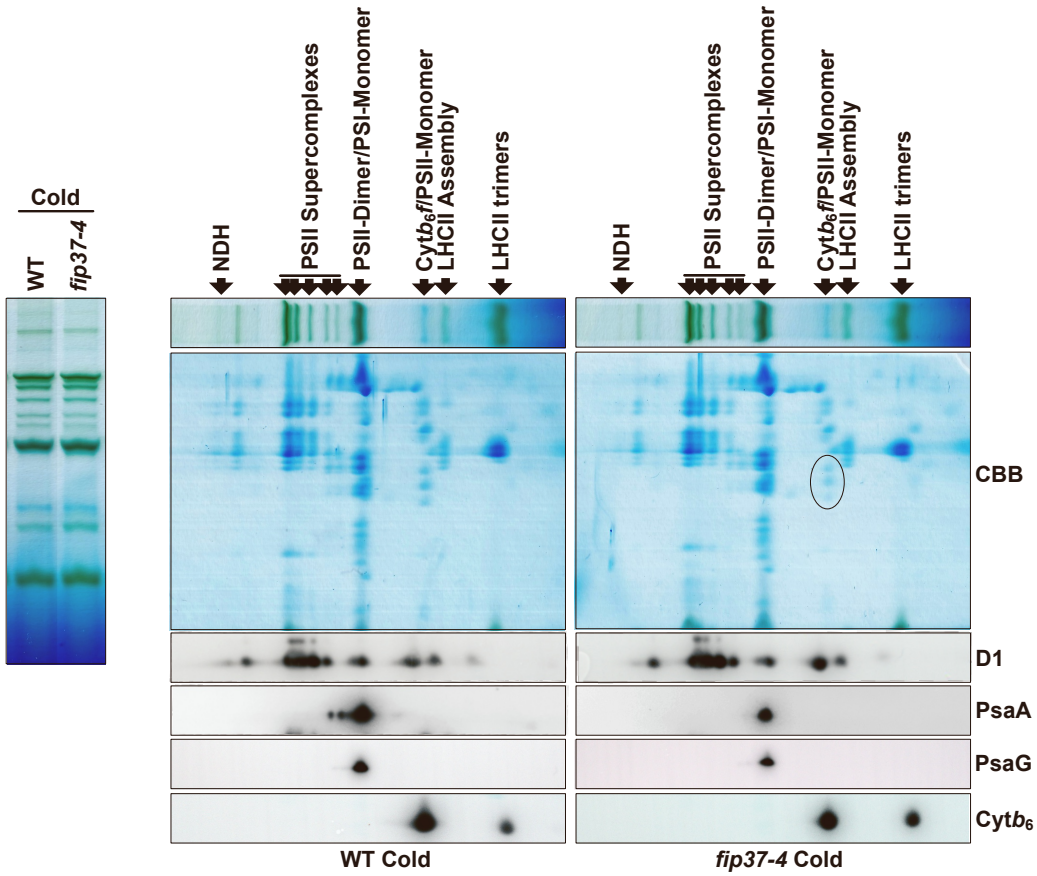

Supplemental Figure S4. Analysis of thylakoid membrane complexes using BN-PAGE

Loading of thylakoid complexes was based on equal amount of chlorophyll. The first dimension was performed using BN-PAGE of solubilized thylakoid membrane complexes of WT and mutant plants grown under cold conditions (left part). The appearing protein complexes are indicated (right upper part). Proteins in the second dimension were stained with Coomassie Brilliant Blue (CBB) (right middle part). The Cytb_6f complex is circled. The second dimension was subjected to immunodecoration using D1, PsaA, PsaG, and Cytb_6 sera (right lower part).

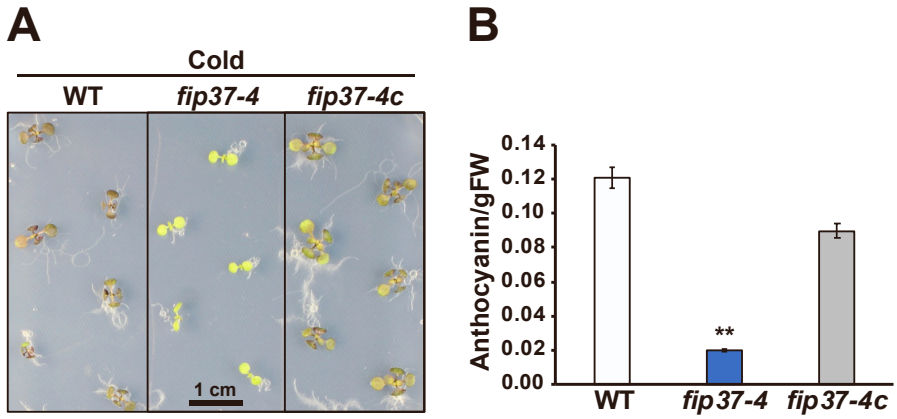

Supplemental Figure S5. FIP37 is important for anthocyanin production in the cold (A) Phenotype of WT, *fip37-4,* and *fip37-4c* grown in vitro at 22°C for 7 days followed by a shift to 4°C for 30 days.

(B) Anthocyanin content in WT, *fip37-4,* and *fip37-4c* after cold treatment. 15 replicates for each genotype were measured. Statistical significance was determined using Tukey HSD. ** corresponds to a p-value ≤ 0.01. Fresh weight: FW. Scale bar: 1 cm.

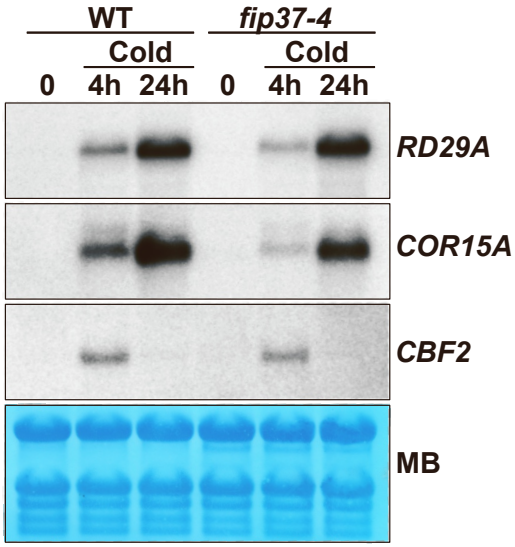

Supplemental Figure S6. Reduced levels of FIP37 has no significant impact on the expression of cold-responsive genes

RNA gel blot analysis of *CBF2*, *COR5A,* and *RD29A* genes in the WT and *fip37-4* before (time 0) and after 4 and 24 hours of cold treatment. 8 µg of RNAs from leaves were used. Methylene blue (MB) was used as loading control.

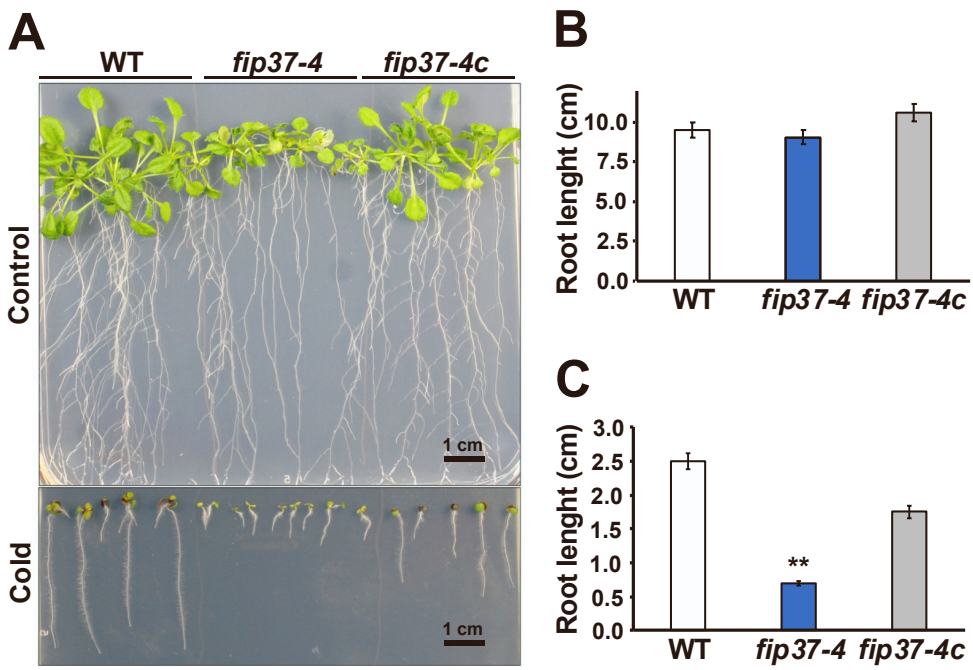

Supplemental Figure S7. Cold-sensitive root growth in *fip37-4*

(A) Phenotype of WT, *fip37-4,* and *fip37-4c* grown vertically on MS medium for 21 days under control conditions (upper part) and after germination for 30 days at 4°C (lower part). Scale bar: 1 cm.

(B and C) Graphs show root lengths of plants grown under control **(B)** and cold **(C)** conditions. 25 replicates for each genotype were measured. Statistical significance was determined using Tukey HSD. ** corresponds to a p-value ≤ 0.01.

Supplemental Table S1. List of putative epitranscriptomic players with chloroplast localization or functional association

The functions of potential epitranscriptomic factors were retrieved from TAIR, INTERPRO, or the STRING database (arabidopsis.org, ebi.ac.uk, string-db.org, respectively). The putative subcellular localization was estimated by ARAMEMNON (aramemnon.uni-koeln.de). The consensus score AramLocCon is indicated. The tissue with highest expression levels was taken from the Arabidopsis eFP Browser (http://bar.utoronto.ca). The DOI numbers of latest references (TAIR) dealing either specifically or generally with the factors is listed. Interaction partners were predicted using the STRING and the Biogrid (thebiogrid.org) database.

Gene name	Tentative function	Subcellular localisation and consensus score	Mainly expressed in:	References/DOI	Interactions
black, writers **red, readers** **blue, erasers**	**Interpro (www.ebi.ac.uk)** **String (string-db.org)** **TAIR (arabidopsis.org)**	**AramLocCon (aramemnon.uni-koeln.de)** **c, chloroplast** **m, mitochondrium** **n, nucleus**	**Arabidopsis eFP Browser (http://bar.utoronto.ca)**	**TAIR (arabidopsis.org)**	**String (string-db.org)** **Biogrid (thebiogrid.org)**
AT1G01860	PFC1, chloroplast Ribosomal RNA adenine dimethylase family protein	c 21.1	Leaves	10.1105/tpc.10.5.699	AT4G26600, methyltransferase activity, RNA binding; Involved in rRNA processing; AT3G13230, RNA-binding KH domain-containing protein; AT3G11964, rRNA biogenesis protein *rrp5*
AT1G06560	putative NSUN 5-methylcytosine RNA methyltransferase (AtNOP2c); rRNA processing	c 1.9, n 3.9	Leaves	10.1186/s12870-017-1206-0	AT5G04600, RNA-binding (RRM/RBD/RNP motifs) family protein
AT1G12800	chloroplast localized S1 RNA binding protein, OB-fold-like protein	c 21.8	Leaves	10.1111/tpj.12889	At1G63310, Uncharacterized protein; AT1G06720, GTPase activity; Involved in ribosome biogenesis; AT3G06530, Involved in ribosome biosynthesis ; AT4G04940, Transducin family protein / WD-40 repeat family protein; Its function is described as nucleotide binding
AT1G31600	RNA-binding (RRM/RBD/RNP motifs) family protein	c 1.9, n 3.7	Leaves	10.1093/nar/gkr406	At1G78190, Multifunctional methyltransferase subunit TRM112-like protein; Acts as an activator of both RNA and protein methyltransferases

AT1G32360	RNA binding zinc finger (CCCH-type) family protein	n 8.5	Leaves, seeds	10.3390/ijms2303 1572	AT2G04080, MATE efflux family protein; AT5G13570, mRNA-decapping enzyme subunit 2
AT1G36310	S-adenosyl-L-methionine-dependent tRNA methyltransferases superfamily protein	c 4.8, m 8.6	Leaves	10.1093/nar/gkr40 6	At1G78190, Acts as an activator of both RNA and protein methyltransferases
AT1G45110	Ribosomal RNA small subunit methyltransferase I (RsmI)	c 9.4, m 11.5	Leaves	10.1104/pp.105.0 66290	At5G10620, Putative plastid RNA methyltransferase; AT2G02740, WHIRLY 3, plastid, DNA binding
AT1G50000	RNA Methyltransferase; Involved in rRNA processing	c 16.6, m 11.4	Leaves	10.1093/jxb/erx08 2	AT5G53920; Ribosomal protein L11 methyltransferase-related; AT1G45110, 16S rRNA (cytidine1402-2'-O)-methyltransferase
AT1G55500	putative mRNA methylation-of-N6-adenosine reader protein (AtECT4)	c, 0.2, n 6.6	Flowers, meristem, leaves	10.1080/1559232 4.2022.2079308; 10.1242/dev.1891 34	AT3G27700 and AT1G21580; RNA recognition motif (RRM)-containing protein; Its function is described as RNA binding, nucleotide binding, zinc ion binding, nucleic acid binding; AT3G54170, FIP37; AT4G10760, MTA
AT1G60230	putative (bacteria RlmN/CFR)-like dual-specificity rRNA & tRNA methyltransferase	c 14.7, m 7.5	Leaves	10.1093/jxb/erx08 2	AT4G01850, S-adenosylmethionine synthetase 2
AT1G69523	S-adenosyl-L-methionine-dependent methyltransferases superfamily protein	c 16.9; n 2.4	Leaves	10.1104/pp.108.1 21038	AT1G71370, DEA(D/H)-box RNA helicase family protein; AT5G64150, RNA methyltransferase family protein; AT5G05450, P-loop containing nucleoside triphosphate hydrolases superfamily protein. Its function is described as helicase activity
AT1G69526	S-adenosyl-L-methionine-dependent methyltransferases superfamily protein	c 13.7, 11.5	Seeds	10.1104/pp.108.1 21038	AT5G64150, RNA methyltransferase family protein; AT3G17390, S-adenosylmethionine synthetase family protein

AT1G78010	tRNA modification GTPase MnME	c 15.2, m 10.4	Leaves	10.3389/fpls.2014.00678	AT2G13440, Involved in tRNA processing; AT1G51310, tRNA (5-methylaminomethyl-2-thiouridylate)-methyltransferases
AT2G13440	tRNA uridine 5-carboxymethylamino methyl modification enzyme MnmG-related	c 21.4; m 8.7	Leaves	10.1074/jbc.M308435200	AT1G78010, tRNA modification GTPase; AT1G51310, tRNA (5-methylaminomethyl-2-thiouridylate)-methyltransferase activity
AT2G17970	RNA demethylase ALKBH9B/ALKBH 10B-like	n 9.1	Leaves, flowers, meristem	10.3389/fpls.2021.701683	AT4G09980, Methyltransferase MT-A70 family protein; FIP37; AT4G35910, Plays a central role in 2-thiolation of mcm(5)S(2)U at tRNA wobble positions of tRNAs
AT2G19870	tRNA/rRNA methyltransferase (SpoU) family protein	c 13.6, m 11.2	Nd	/	AT4G25730, Adomet-dependent rrna methyltransferase spb1; AT1G54310, S-adenosyl-L-methionine-dependent methyltransferases superfamily protein; Its function is described as RNA binding; AT5G18570, Functions in the biogenesis of thylakoid membrane and plastid ribosome during chloroplast development; AT4G25730, Probable methyltransferase involved in the maturation of rRNA and in the biogenesis of ribosomal subunits
AT2G22090	RNA-binding (RRM/RBD/RNP motifs) family protein	c 7.7; n 7.0	Leaves, seeds, flowers	10.3390/biom10040661	AT3G56860, Heterogeneous nuclear ribonucleoprotein (hnRNP)-like protein that acts as component of a complex regulating the turnover of mRNAs in the nucleus; AT5G64270, RNA binding splicing factor, putative; AT2G38610, RNA-binding KH domain-containing protein; AT4G11420, RNA-binding component of the eukaryotic translation initiation factor 3
AT1G32360	Zinc finger (CCCH-type) family protein of the m6A writer complex, interacts with HAKAI	n 8.5	flowers, seeds, leaves	10.3390/ijms23031572	AT1G08370 and AT5G13570, mRNA-decapping enzyme-like proteins; AT5G42810, Inositol-pentakisphosphate 2-kinase
AT2G39670	Ribosomal RNA large subunit methyltransferase RlmN/Cfr	c 21.2, m 3.0	Leaves, meristem	/	AT1G12800, RNA-binding, OB-fold-like protein; AT2G39670, RNA methyltransferase activity; Involved in rRNA processing; several chloroplast ribosomal RNAs

AT2G41040	S-adenosyl-L-methionine-dependent methyltransferases superfamily protein	c 31.2	Flowers	/	AT5g03900 and AT1g16080, Uncharacterized proteins; AT1G12250, uncharacterized pentapeptide repeat-containing protein; AT5G13650, putative chloroplastic elongation factor involved in response to chilling stress.
AT3G13060	contains YTH (YT521-B homology), an evolutionarily conserved m^6A-dependent RNA binding domain	c 2.7; n 5.5	Leaves	10.3390/biom10040661	AT1G02080, Transcription regulator; AT4G00660, DEAD-box ATP-dependent RNA helicase; AT3G27700, RNA recognition motif (RRM)-containing protein; AT1G16210, Uncharacterized protein
AT3G13180	RNA (C5-cytosine) methyltransferases	c 20.9; m 6.9	Leaves	10.1186/s12870-017-1206-0	AT3G13180, NOL1/NOP2/sun family protein / antitermination NusB domain-containing protein; Its function is described as RNA binding; AT5G15550, Transducin/WD40 repeat-like superfamily protein; Required for maturation of ribosomal RNAs; AT5G04600, RNA-binding (RRM/RBD/RNP motifs) family protein
AT3G13460	The YTH (YT521-B homology) domain has been suggested to be an evolutionarily conserved m6A-dependent RNA binding domain	c 1.3; n 3.6	Meristem, seeds, leaves	10.7554/eLife.72375	AT2G25090, CIPK, CBL-interacting serine/threonine-protein kinase 16; AT5G21140, Uncharacterized protein; AT4G38600, HEAT repeat, HECT-domain (ubiquitin-transferase)
AT3G21300	(Uracil-5)-methyltransferase family	c 6.3; m 13.3	Leaves	10.3390/biom10040661	AT3G15460 and AT1G52930, Ribosomal rna processing brix domain protein; AT3G13230, RNA-binding KH domain-containing protein
AT3G23830	Glycine-rich RNA-bindingzZinc finger (CCCH-type)protein, induced by cold	c 11.8; m 8.5	Meristem	10.1007/s10930-013-9504-3	AT3G03920, Putative H/ACA ribonucleoprotein complex; AT1G52930, Ribosomal rna processing brix domain protein; AT4G29510, Methylates (mono and asymmetric dimethylation) the guanidino nitrogens; AT4G12600, RNA binding ribosomal protein L7Ae; AT1G52930, Ribosomal rna processing brix domain protein
AT3G28460	RsmD, chloroplast RNA methyltransferase	c 22.9	Leaves	10.1093/pcp/pcab060	AT4G26370, Antitermination NusB domain-containing protein; Its function is described as RNA binding;

					AT4G39040, RNA-binding CRS1 / YhbY (CRM) domain protein; Its function is described as RNA binding; AT5G46420, 16S rRNA processing and ribosome binding protein RimM family
AT3G56330	tRNA methyltransferase, Trm1	c 15.8	Leaves	10.1371/journal.pone.0242737	AT5G24840, tRNA (guanine-N(7)-)-methyltransferase; AT5G13830, FtsJ-like methyltransferase family protein; AT1G15440, Periodic tryptophan protein 2; Involved in nucleolar processing of pre-18S ribosomal RNA; AT5G14520, Pescadillo-like protein; Required for maturation of ribosomal RNAs and formation of the large ribosomal subunit
AT4G01880	Trm13 is a tRNA methylase that catalyzes 2'-O-methyladenosine (Am) nucleoside formation on tRNA(Gly)(GCC)	c 4.2; m 5.6	Leaves, meristem, flowers	10.1186/s12870-017-1206-0	AT4G17610, tRNA/rRNA methyltransferase (SpoU) family protein; AT3G26410, nucleic acid binding methyltransferases; AT5G01230, S-adenosyl-L-methionine-dependent 2'-O-ribose methyltransferases superfamily; AT1G36310, S-adenosyl-L-methionine-dependent methyltransferases
AT4G02940	putative DOXA class oxidative mRNA demethylase (AtALKBH10b)	c 7.0; m 3.7; n 3.3	Leaves, flowers	10.1186/s13059-022-02814-8	AT4G35910, Adenine nucleotide alpha hydrolases-like superfamily protein; AT3G54170, FIP37; AT4G09980; m6A methyltransferase MTA
AT4G04880	N6-mAMP deaminase (ADAL, renamed MAPDA)	Nd	Leaves, flowers	10.1080/15476286.2019.1642712	AT3G26410, tRNA methyltransferase activity; AT4G18905, Transducin/WD40 repeat-like superfamily protein, its function is described as nucleotide binding
AT4G24770	31-kDa RNA binding protein	c 26.9	Leaves	10.1093/jxb/erab165	AT1G78630, 50S ribosomal protein L13, chloroplastic; AT4G26370, Antitermination NusB domain-containing protein, its function is described as RNA binding; AT3G12930, Protein Iojap, chloroplastic; May be a ribosome silencing factor; AT3G20930, RNA-binding (rrm/rbd/rnp motifs) family protein
AT4G34110	PAB poly(A) binding protein 2	c 5.7	Leaves, flowers, meristem	10.1186/s13059-019-1799-8	AT1G18070, Translation elongation factor EF1A; AT1G54170, Polyadenylate-binding protein-interacting protein 3; AT4G00660, DEAD-box ATP-dependent RNA helicase 8; AT5G44200, Nuclear cap-binding protein subunit 2

AT4G38020	tRNA/rRNA methyltransferase (SpoU) family protein	c 9.3; m 3.4	Leaves	/	AT1G54310, S-adenosyl-L-methionine-dependent methyltransferases; AT1G35680, 50S ribosomal protein L21 and L3-1; AT3G04820, Pseudouridine synthase; AT3G25920, 50S ribosomal protein L15; AT2G41670, P-loop containing nucleoside triphosphate hydrolase
AT5G10620	RNA methyltransferase RlmH	c 19.5	Leaves, flowers	/	AT5G53920, Ribosomal protei n L11 methyltransferase-related; AT1G45110, 16S rRNA (cytidine1402-2'-O)-methyltransferase; AT5G50110, S-adenosyl-L-methionine-dependent RNA methyltransferases; AT5G10910, S-adenosyl-L-methionine-dependent methyltransferase, MraW; AT5G24840, tRNA (guanine-N(7)-)-methyltransferase
AT5G10910	CMAL, chloroplast mraW m4C methylase family protein	13.1; m 11.6	Leaves, meristem	10.1093/nar/gkaa129	AT1G64600, Methyltransferases;copper ion binding, contains Ribosomal protein Rsm22; AT1G49400, Uncharacterized protein; AT2G15820, Pentatricopeptide repeat-containing protein; AT1G79850, Plastid ribosomal small subunit protein 17; AT5G64580, Required for plastid development during embryogenesis
AT5G11530	Zinc finger (CCCH-type) family protein	n 7.8	Seeds	10.1073/pnas.1920621117	AT5G64360, Chaperone DnaJ-domain superfamily protein, its function is described as heat shock protein binding; AT5G58230, Transducin/WD40 repeat-like superfamily protein
AT5G15390	tRNA/rRNA methyltransferase (SpoU) family protein	c 19.6; m 3.2	Leaves	/	AT1G54310, S-adenosyl-L-methionine-dependent methyltransferase; AT4G10650, P-loop containing nucleoside triphosphate hydrolases superfamily protein; AT5G26180, S-adenosyl-L-methionine-dependent methyltransferases superfamily protein
AT5G17660	tRNA (guanine-N-7) methyltransferase	c 24.1; n 2.2	Leaves, flowers	/	AT5G14600, tRNA (adenine-N1-)-methyltransferase; AT2G22400, RNA methyltransferase; AT5G15810, tRNA (guanine(26)-N(2))-dimethyltransferase 1
AT5G26180	S-adenosyl-L-methionine-dependent methyltransferases superfamily protein	c 7.5; m 6.6	Meristem, leaves	10.3390/biom10040661	AT3G16810, Pumilio (APUM) proteins containing PUF domain (eight repeats of approximately 36 amino acids each). PUF proteins regulate both mRNA stability and translation through sequence-specific binding to the 3' UTR of target mRNA transcripts; AT5G04600, RNA-binding (RRM/RBD/RNP motifs) family protein;

					AT2G40360, Transducin/WD40 repeat-like required for maturation of ribosomal RNAs; AT3G22660, Probable rRNA-processing protein EBP2 homolog
AT5G50110	Ribosomal RNA small subunit methyltransferase G [rsmG]	c 10.3; m 8.9	Leaves, flowers, meristem	/	AT1G78010, tRNA modification GTPase; AT3G20557, Hypothetical protein; Involved in the regulation of plant growth
AT5G58190	YTH (YT521-B homology), evolutionarily conserved m6A-dependent RNA binding domain	c 10.3; n 6.6	Leaves, flowers, meristem	10.3390/biom10040661	AT1G02080, transcription regulator activity; AT2G27100, cap-binding complex (CBC) and both the pre-mRNA splicing and primary microRNAs (miRNAs) processing machinery; AT1G54440, Polynucleotidyl transferase, ribonuclease h fold protein
AT5G61020	ECT3 - Evolutionarily conserved C-terminal region 3 (ECT3); YTH domain	n 6.8	Meristem, flowers	10.1080/15592324.2022.2079308	AT3G27700, RNA recognition motif (RRM)-containing protein; AT2G39580, Putative zinc-finger domain; AT5G14520, NOP56-like pre RNA processing ribonucleoprotein
AT5G66360	Ribosomal RNA adenine dimethylase family protein	m 11.9; n 9.2; c 1.6	Petioles	10.1105/tpc.10.5.699	AT3G13230, RNA-binding KH domain-containing protein, its function is described as RNA binding; AT4G26600, RNA methyltransferase activity

Supplemental table S2. List of oligonucleotides used in this study. Sequences are shown in 5' → 3' direction

NAME	Sequence	Purpose
ACTIN_FWD	CTTGCACCAAGCAGCATGAA	qRT PCR
ACTIN_REV	CCGATCCAGACACTGTACTTCCTT	qRT PCR
ZAT12_FWD	AAGAAGCCTAACAACGACGC	qRT PCR
ZAT12_REV	AACAAAGCGCGTGTAACCAA	qRT PCR
ZAT10_FWD	CACAAGGCAAGCCACCGTAAG	qRT PCR
ZAT10_REV	TTGTCGCCGACGAGGTTGAATG	qRT PCR
SOD_FWD	CTGGTCCACATTTCAACCCC	qRT PCR
SOD_REV	CTTTCCGAGGTCATCAGGGT	qRT PCR
APX1_FWD	TAGGTCTGGCTTCGAAGGTG	qRT PCR
APX1_REV	CAGCAGCGTATTTCTCGACC	qRT PCR
CBF2_FWD	GGCTCCGATTACGAGTCTC	Probe for RNA gel blot
CBF2_REV	GCTCCATAAGGACACGTCATC	Probe for RNA gel blot
RD29A_FWD	CACACCAGCAGCACCCA	Probe for RNA gel blot
RD29A _REV	CCGAGAACAGAGTCAAAGTCC	Probe for RNA gel blot
COR15A_FWD	GGCGATGTCTTTCTCAGGAG	Probe for RNA gel blot
COR15A _REV	GTGGCATCCTTAGCCTCTC	Probe for RNA gel blot
MTA PROBE_FWD	ATGGAAACTGAATCTGATGACGC	Probe for RNA gel blot
MTA PROBE_REV	CTCTTTGCTATGGTTGAGCC	Probe for RNA gel blot
MTB PROBE_FWD	GAGCATCAAGATCGTGATTCC	Probe for RNA gel blot
MTB PROBE_REV	CCAGGAGGTCCACCACC	Probe for RNA gel blot
HAKAI PROBE_FWD	GAGGGATTCCCCGACGG	Probe for RNA gel blot
HAKAI PROBE_REV	GACCGTCTCTACCCCGG	Probe for RNA gel blot
PSAD_ FWD	CCCAAATCCCTCTCCTTCAC	Probe for RNA gel blot
PSAD_ REV	CCTTCTCTTCCTGGATTCGC	Probe for RNA gel blot
PSAL_FWD	CAAAATTCATATCCCTGAGAGCCACAAC	Probe for RNA gel blot
PSAL_REV	TTGACGAAGTAAGGAAGGTCAAGAACG	Probe for RNA gel blot
PETC_FWD	ATGGCGTCCTCATCCCTTTCC	Probe for RNA gel blot
PETC_REV	GACCACCATGGAGCATCACCA	Probe for RNA gel blot
ACTIN PROBE_FWD	ATGGCTGATGGTGAAGATATTC	Probe for RNA gel blot
ACTIN PROBE_REV	CGGTGAACAATCGACGGG	Probe for RNA gel blot
PSAA_80-MER	CCACATCTCCATTCAGGATTTCTTGGCCCACT ATTGGCCAAACCACCTGAGCACTAGGTCCA ATGTGAGTAGGATCACTC	Probe for RNA gel blot
PSAO_80-MER	ATCTCTCCTCAACCAGTTCCTCTCAAAGCA AGTGACTCTTCCTCCCGATGCACCGGCGAGTCT CAAAGGGTTCTTGGCGC	Probe for RNA gel blot
PSBO_80-MER	CGTACGTTAGCCTCTTTGGTGCTCCC TCCGCACCGGCCCCCGAGACAACGAGA GCAGAGGTGGCTAGAGCAAAACCGGCG	Probe for RNA gel blot

PETB_80-MER	ACTCATATTCCGGAAATATACAATGCA GAAAAAAATTTCGCGGTCGAACTACCA AAGGAGAATAGGCTAAAATTGTTAGA	Probe for RNA gel blot
PSBA_80-MER	GTTTCCCTGATCAAACTAGAAGTTACC AAGGAACCATGCATAGCACTAAAAAGGGAG CCGCCGAATACACCAGCTACACC	Probe for RNA gel blot